Czochralski growth of metal single crystals

Aloufri, Majed Saeed

CZOCHRALSKI GROWTH OF METAL SINGLE CRYSTALS

BY

MAJED SAEED ALOURFI

(King Abdulaziz University, Jeddah, S.A.)

A thesis submitted to the University of Durham for
the Degree of Master of Science

Department of Physics,
University of Durham, U.K.

August, 1986.

CONTENTS

ABSTRACT

This work aims to produce metal single crystals by the Czochralski technique. Single crystals of copper, aluminium and nickel were grown by this technique. The Laue method was used to confirm that these crystals are single. Nickel single crystals were examined by using synchrotron radiation in both transmission and reflection. Magnetic domain and dislocation bands could be seen. A theoretical study has also been carried out, following Buckley-Golder, to find the effect of the seed, neck and crystal dimension on the temperature gradient in the reduction of thermal stress and consequent dislocation density.

PREFACE

In the last decade the growth of single crystals has become very important, because the intrinsic properties of a material cannot be properly obtained until high purity and perfect single crystal specimens have been prepared.

The process of crystal growth can be divided into four main categories: solid growth, vapour growth, solution growth and melt growth.

Czochralski method has been used to grow zero-dislocation density semiconductor material such as silicon (Dash, 1958), and germanium (Okkerse, 1959). With respect to metals, the problem is more difficult, due to the lower energy of formation of dislocation in metals than in semiconductors (Elbaum, 1960). However, there are some metals which were grown free from dislocations by this method such as silver (Tanner, 1973) and copper (Sworn and Brown, 1972).

The aim of this work is growing high quality single crystals of nickel by the Czochralski technique. The reason for this, which is a part of a joint project with the University of Strathclyde, is to study in situ the hydridation of nickel since it causes precipitation of the hydride phase due to a high solubility of small hydrogen atoms. Producing a high quality single crystal of nickel will enable the researcher to study the substructure in a dynamical situation as the hydridation takes place. He will also be able to examine the defect structure

change due to mechanical deformation, and investigate how the internal defect structure relates to hydride decomposition.

Chapter One is a review of crystal growth from the melt. Chapter Two is a brief review of crystal growth by other methods, solid growth, vapour growth and solution growth. Chapter Three reviews X-ray topography. Chapter Four investigates some applications of the X-ray topography technique. Chapter Five is a theoretical study based on the model of Buckley-Golder and Humphreys of the effect of geometric changes in the seed, neck and crystal dimension on the temperature gradient. In Chapter Six the production of single crystals of metals by the Czochralski technique is discussed while Chapter Seven presents the results of the present study.

ACKNOWLEDGEMENTS

I would like to express my gratitude to my Supervisor, Dr. B.K. Tanner, for his guidance, assistance, encouragement and invaluable suggestions throughout this work. I also wish to thank Dr. W.D. Corner for his interest and encouragement.

I would like to thank Professor A.W. Wolfendale, F.R.S., and Professor B.H. Bransden for the use of the facilities of the Physics Department.

I am grateful to all the members of the Solid State Group, both past and present, for their friendly co-operation. In particular, I would like to thank Mr. D.B. Lambrick, Mr. N. Loxley and Dr. M. Surowiec. I would like to thank Mr. D. Oliver for his helpful assistance in the technical aspects of this work.

I wish to thank Dr. A.A. Goharji for the help he has given me in computing, and I would like to thank Mrs. M.A. Chipchase for typing this thesis.

Financial support from King Abdulaziz University, Jeddah, Saudi Arabia, is gratefully acknowledged.

Finally, I wish to express my sincere thanks to my Mother for her moral support.

CHAPTER ONE

CRYSTAL GROWTH FROM THE MELT

1.1 Introduction

Growth from the melt, of which the principal techniques are Czochralski, Bridgman and Float Zone techniques, is the most widely used process for the preparation of single crystals.

Any material can be used to grow single crystals from the melt provided the material melts congruently, does not decompose before it melts and does not undergo a structural change during cooling.

1.2 Czochralski growth

Undoubtedly one of the most important growth techniques is the pulling technique which is named after Czochralski.

The main advantages of this method are that it is generally a quick crystal growing method, it has good visibility enabling the necking process to be controlled, and that the crystal size can be controlled. This method of producing single crystals will be discussed in Chapter six.

The important difference between this method and other melt-growth methods are that the crucible does not act as a mould and the liquid solid interface is not in contact with the crucible (Jones 1974).

The advantage of the Czochralski technique over the Float Zone is that large crystals can be grown, whereas Float Zone growth is limited to small crystals.

The main disadvantage of this method is that we have to melt our charge in a crucible which may act as a source of contamination.

The criteria that must be fulfilled for successful pulling have been listed (Laudise, 1970) as follows.

i. The crystal should not react with the crucible or the atmosphere during growth.

ii. The crystal should melt congruently without decomposition.

iii. The melting temperature of the charge should be obtainable by using a variable heater.

iv. It should be possible to establish a combination of pulling rate and thermal gradients where single crystal material can be formed.

1.2.1 Liquid Encapsulation Czochralski (LEC)

This technique (Brandle, 1980) is used to overcome one of the main material limitations of the Czochralski technique, namely that material should have low vapor pressure. In this method (Figure 1.1) the charge is placed inside the crucible with the B_2O_3 encapsulant. As the power increases, the B_2O_3 melts coating the charge. When the charge is melted the B_2O_3 forms a liquid layer above the molten charge. The growth process is begun and the control diameter can be made manually or automatically. This method has been used by Fang et al. (1984) to grow InP single crystals with various dopents S, Sn, Zn and Fe. They reported that dislocation free Zn-doped p-InP single crystals have been obtained.

Fully encapsulated Czochralski (FEC), (Figure 1.2), has been used by Kohda (1985) to grow zero dislocation density GaAs. In this method, the crystal grown is wholly encapsulated in liquid B_2O_3. The stress induced by arsenic evaporation from the crystal surface resulting in surface irregularities is suppressed and therefore reduced.

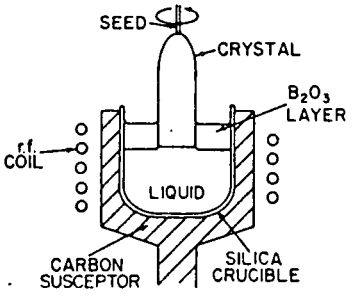

LEC crystal pulling arrangement.

Figure 1.1 (after Brandle 1980)

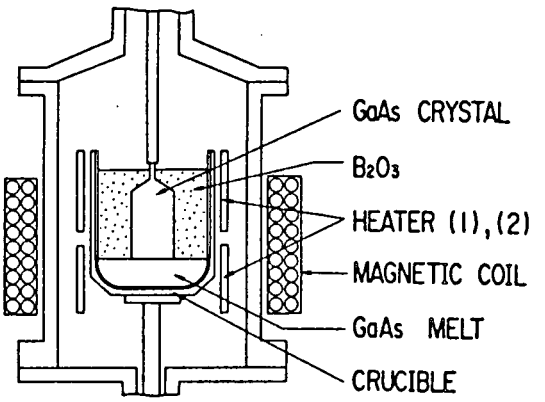

Growth apparatus for the VM-FEC method.

Figure 1.2 (after Kohda, 1985).

1.2.2 Diameter control

Paige (1983) described seven methods for the diameter control grown by this technique.

1.2.2.1 The "bright ring" method When an optical pyrometer focused on the melt surface around the crystal was used, changes in the crystal diameter were detected as meniscus, bright ring, advanced or retreated across the view of the pyrometer increasing or decreasing its output. Thus a constant pyrometer output is obtained by adjusting crystal diameter (Paige, 1983).

1.2.2.2 The melt level method In this method, the differential of the melt level with respect to crystal length or pull rate gives the crystal diameter (Paige, 1982). This method was used by Goniletsky et al. (1981) to grow Kcl single crystals and the diameter control was within $\pm$ 1.5%.

1.2.2.3 The X-ray shadow method This method was used by Van Dijk et al. (1974) to control the diameter of Gallium phosphide single crystals which were grown by the liquid encapsulated Czochralski (LEC) technique using a television monitor. They were able to pull crystals with 2.0 $\pm$ 0.5 mm diameter. This method was also used by Pruatt and Lien (1974) to grow a uniform diameter of Gallium phosphide single crystal by LEC technique. In this method a point source of X-rays is used to produce a shadow image of the growing crystal on a fluorescent screen. The shadow image is converted into a visible image displayed on a TV monitor by using a high-sensitivity TV camera.

1.2.2.4 The otpical TV imaging method. This method was described by Gartner et al. (1972). The television camera produces an intensity profile scan as a video image. The video - signal of the crystal which is proportional to the diameter is fed into the reference input of the RF power control system. The diameter control was ± 0.3% during crystal growth. This method was also used by O'Kane et al. (1972) to grow single crystals of $(KNbO_3)_{10}$, $(LiNbO_3)_{35}$ and $(BaNb_2O_6)_{55}$.

1.2.2.5 The Laser reflection method. This technique was described by Gross and Kersten (1972). They were able to grow Potassium chloride and a bismuth germanium oxide and the crystal diameter was constant within about 1%. In this method, the laser beam, reflected from the melt surface near the growing interface, is detected by two photodiodes and is related to the crystal diameter. The signals which come from them are amplified, rectified and subtracted from each other. The different voltage is proportional to the deviation of the crystal diameter from its desired value.

1.2.2.6 The weighing method. This method was used by Bardsley (1972) to control the diameter of Sodium Chloride and germanium single crystals. The control with NaCl was ± 2% over 10 cm crystal length. In this method the length of the crystal is determined from the withdrawal mechanism travel. For a constant diameter of the crystal, the length of the crystal is in a fixed proportion to the loss of the melt weight. When the diameter is incorrect the proportion changes and an error signal is generated and fed back to the R-F generator control system. This result

in a change in the melt temperature and consequently a desired crystal diameter is grown.

1.2.2.7 Viscous torque This method was used by Paige (1983) at Durham University. It involves the measurement of the viscous torque on the crystal as it revolves in the melt to determine the size of the crystal. The crystal diameter is varied by varying the melt temperature.

1.2.3 Some previous uses of this method

This method has been used to grow zero dislocation density silicon single crystals by Dash (1958) who in (1959) explained the source of dislocations occurring during the crystal growth and how it could be eliminated.

Steinemann and Zimmerli (1966) reported they were able to produce zero dislocation density GaAs by this method. They state that neck should be present before growing the crystal and new dislocation will be generated if any impurity exist.

Zuleher and Huber (1982) grew silicon single crystals with zero dislocation density. They state that the oxygen content is strongly influenced by the crystal and crucible rotation. The oxygen content increased with isorotation but was reduced with counterrotation.

Dislocation free Germanium crystals were grown by this method by Okkerse (1959). He found that the neck has a marked effect on the quality which is also affected by the purity of the melt.

1.3 The Bridgman Technique

This method was used first by Bridgman and then developed by Stockbarger and is known as the Bridgman-

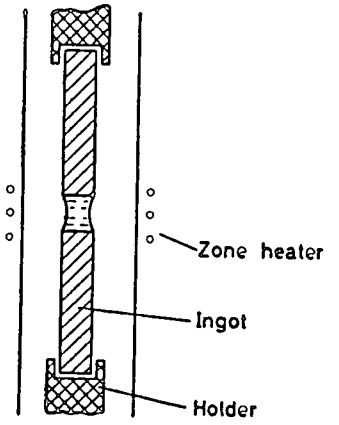

Figure 1.3 Floating zone technique
(after Lawson and Nielsen, 1958).

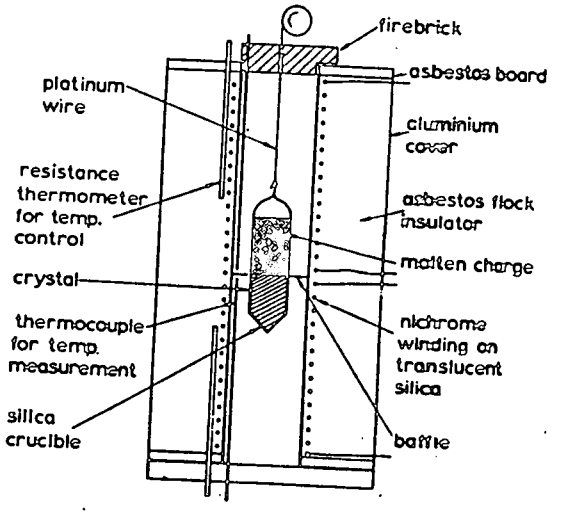

Figure 1.4 (after Brice 1965).

Stockbarger method (Loudise, 1970).

The basic concept in Bridgman technique is that the whole charge is melted first and then solidified from one end, where a seed crystal can be located if necessary. A window should be available to check that the seed has been partially melted (Brice 1965). The method uses a vertical arrangement or horizontal arrangement. In the vertical method the melt in the crucible is made to solidify from the lower end of the crucible by lowering the crucible or moving the furnace. The advantage of this method is the variety of size of crystals which can be produced, because it is fixed by crucible geometry (Jones 1974). On the other hand this method cannot be used for semi-conductors because they expand on solidification and produce a large stress on the crucible which acts as a constraint (Loudise, 1970).

To produce a good crystal, the lowering rate should be slow to keep the solid/liquid interface planar and to avoid polycrystalline ingot formation due to rapid cooling, (Lawson and Nielsen, 1958). Also the horizontal method can be used with the advantage that its arrangement is simple, and the disadvantage that the contamination is increased due to the wide open surface.

1.3.1 Some previous uses of this method. Copper single crystals with low dislocation density have been grown by Bridgman technique (Young and Savage 1964). They obtained crystals with a low dislocation density, and the slices cut from the large crystals were annealed. If the dislocation density is more than 10^5 cm^{-2}, there

will be no reduction in the dislocation density, but if it was less than 10^5 cm^{-2} the reduction was divided by a factor of 100. They found that the dislocation density is lower when the growth direction is (111) also, by thinning the crucible wall from .95 cm to .24 cm, the dislocation density would be lowered ten times.

The lowest dislocation density obtained was 10^2 cm^{-2} after they annealed the slices of the purest crystal.

Also by this method Pearson (1953), produced Ni single crystals under vacuum in an alumina sheet crucible. He took back reflection Laue photographs to confirm that the crystals were single after electro polishing. The crystal (1" x5/8" diameter) was then electrolytically polished to remove any remaining material on the surface . He cut it in a picture frame, then it was mechanically and electrolytically polished and reannealed to allow its magnetic properties to be properly studied.

Also (Wernick and Davis 1956) managed to grow high purity single crystals of copper by this method under a vacuum in a graphite crucible. They found that a rapid lowering rate led to bicrystals and by lowering it by 2" per hour the perfection was very high.

1.4 Float Zone

The float zone technique is the zone melting technique in a vertical plane. In this method, the seed crystal is held vertically upwards and a polycrystalline ingot downward in such a way that it touches the top of the seed. The zone is moved down through the ingot and where

the seed begins to melt, the direction of the zone is reversed and the seed grows as the zone is moved upwards.

In this method, the melt is in contact only with its own solid. This is obviously an advantage because that will eliminate the possibility of introducing impurities or strain during cooling.

1.4.1 Some previous uses of this method. This technique, where the molten zone is held in place by surface tension between two vertically colinear solid rods was described first by Keck and Colay (1953) to grow single crystal of silicon.

Also Calverley, et al. (1957) state that by this method and using electron bombardment as a heat source they produced single cystals 2 mm to 1 cm in diameter and up to 16 cm long of tungsten, rhenium, tantalum, molybdenum, vanadium, silicon using a seed crystal, and copper, but they were not able to produce single crystals of iron, due to the phase change in cooling, nor in titanium.

Keck et al. (1957) found that the stability of the liquid zone for a specimen of given diameter will decrease as the length of the liquid column increases. So, the zone cannot be supported by surface tension if its length exceeds a certain value.

The horizontal technique has been used by Pfann and Magelbarger (1956). They used an electromagnetic field to support an ingot of silicon. They passed a direct current through a cylindrical ingot which was clamped horizontally at both ends. They applied a magnetic field horizontal to the zone which was to be suspended. They

arranged the direct current and magnetic field to balance the gravitational field. Nickel single crystals were produced by Hutchinsons (1959) by this method.

CHAPTER TWO

OTHER CRYSTAL GROWTH METHODS

2.1 Solid-solid growth method

Metal crystals can be produced by the solid-solid growth method (also known as the recrystallization growth method), by the strain anneal method and by the phase transformation method. The advantage of the solid-solid method is that the specimen comes in a thin sheet which can be used for X-ray topography examination (Champier 1979).

2.1.1 Strain anneal method. Nøst (1965) managed to produce large single crystals of aluminium by the strain anneal method at a very slow cooling rate.

He took aluminium bars and cold-rolled them to a cross section of 1 millimeter by 15 millimeters.

The strips were annealed for a short time. After they were cold-rolled to a cross section of 1 millimeter by 15 millimeters they deformed 3% in tension, then using a saw they were cut into pieces 30 millimeters long. They suspended vertically in the furnace and the temperature rose to $300^{o}C$ and slowly to $440^{o}C$, $14^{o}C$ per hour, then it cooled down slowly to room temperature.

The dislocation density is 5×10^{3} lines per cm^{2} but in a smaller region, the dislocation density is lowered to 2×10^{2} lines per cm^{2}.

Nes and Nøst (1966) found that the cooling rate down to room temperature is a determinative factor. The dislocation density is increased with an increased cooling rate. They state that the lowest dislocation density they obtained was 5×10^{2} lines per cm^{3} for a cooling

rate of $2^{o}C$ per hour.

Also Deguchi et al. (1978) found the same conclusion i.e. that the cooling rate had a marked affect on the quality of the crystal.

2.1.2 Phase transformation method. This method was used by Jourdan et al. (1972) to produce a large single crystal of titanium.

They cut specimens into about 30 x 10 mm^2 and rolled down to .45 millimeters. The specimens were thinned down to .2 millimeter by mechanical and chemical polishing. They were annealed in a high vacuum 5 x 10^{-10}torr for about 3 days in the α phase after briefly being maintained in the β phase. This is carried out first of all at a temperature only slightly below the transition point, then slowly cooled in the furnace to room temperature at a rate of $3^{o}C$ per hour.

2.2 Vapor growth

This technique was reviewed by Branner (1963) as a method for the growth of metals.

2.2.1 Sublimation condensation

There are two types used; closed tube system using a tube or vacuum evaporator and open tube systems (Figure 2.1).

The growth method was used by Dittmar and Neumann (1958) to grow crystal needles of potassium. They were hexagonal in cross section from 5-1 millimeter long.

Also cadmium crystals were grown by condensation on a quartz fibre in an argon diffusion cell which was inserted to serve as a substrate for condensation between two flat plates.

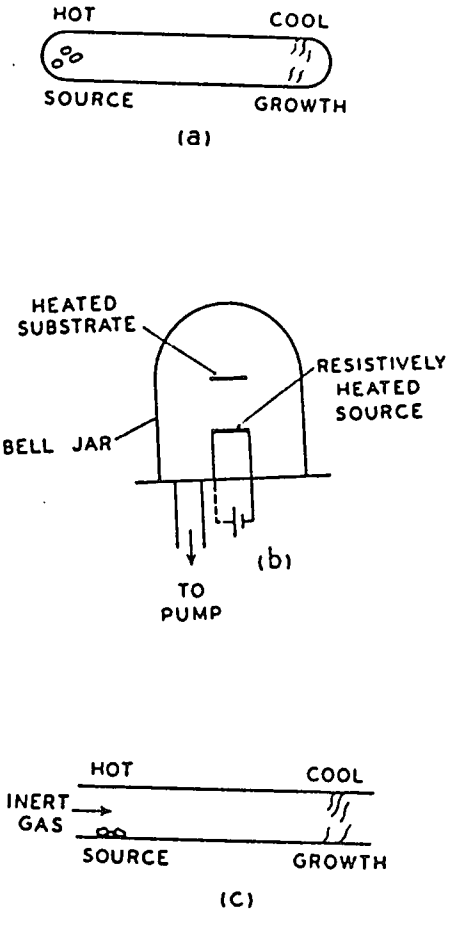

Figure 2.1 Sublimation condensation configuration.
(a) closed tube technique
(b) vacuum evaporation
(c) open-tube technique
(after Landies 1970).

2.2.2 Sputtering.

There are three variants of this technique; cathode sputtering, reactive sputtering and ion implantation, the latter being used for a grown crystal rather than for crystal growth (Laudies 1970).

Theuerer and Heuser (1964) used this technique for growing films of materials such as Nb, Ta, V_3Si, V_3Ge and V_3Ga.

2.2.3 Irreversible reaction.

In this method (Gatog, 1979) where the reaction takes place the reactants are brought into contact with the seed material. This technique is used widely to obtain silicon layers and the reaction which is used is

$$SiHC\ell_3 + H_2 \rightarrow Si + 3HC\ell$$

Theureren (1962) used the hydrogen reduction method for producing an epitaxial film of silicon. He found that the films were single crystals with <111> orientation of the substrate.

2.2.4 Reversible reaction

In this method (Gatog, 1979), the solid material is brought into the vapor phase then under controlled conditions it is reformed by reversing the direction of the reaction. Van Ankel and de Boer used a method of this type to prepare single crystals. This method is called the hot-wire process. This reaction was used to grow Zr

$$Zr(s) + 2I_2(g) \underset{1200}{\overset{450}{\rightleftharpoons}} ZrI_4(g)$$

Cds and Zns single crystals were grown by Greene and Czyzik (1958).

2.3 Crystal growth from solution

2.3.1 Aqueous solution growth. This method (Gatog, 1979) depends on achieving super-saturation without inducing spontaneous nucleation, thus growth can proceed on the seed material. The advantages of this method are its simplicity and that it leads to good quality crystals.

By this method Emara et al. (1969) managed to grow single crystal octahedra of potash alum with a low dislocation density which was investigated by using X-ray topography.

They suspended a small seed crystal in a saturated aqueous solution of pure potash alum at 80°C which was then cooled down to room temperature. A well developed octahedral crystal was formed by adding to the seed after 24 hours.

Also by this technique Duckett and Lang (1973) managed to grow highly perfect hexamethaline tetramine crystals and the best crystals contained very few dislocations.

2.3.2 Flux growth. In this method (Gatog, 1979) supersaturation is obtained by decreasing the temperature of a saturated solution. The seeds can be withdrawn

before the solution is solidified. If seeds are either not used or withdrawn, the solidified flux should be dissolved before the crystal can be recovered.

The difficulty of this technique (Laudies, 1970) is that it requires hard work to find a molten-salt solvent for a given crystal. Also impurity control is another problem if flux components are soluble in the growth crystal.

Using this technique Austermann et al. (1965) managed to grow single crystals of beryllium oxide BeO with low dislocation density. These crystals were grown from lithium molybdate flux at temperatures between $1000^{o}C$ and $1150^{o}C$.

Also Venuteral et al. (1961) grew large single crystals of $Bi_4\ Ti_3\ O_{12}$ bismuth titanate by mixing the 100g of Bi_2O_3 and 5g of TiO_4. He then melted them at $1200^{o}C$ in a platium crucible, and by slow cooling, sheet like crystals at $Bi_4Ti_3O_{12}$ are obtained.

These sheets with intervening Bi_2O_3 layers are easily separated by using a strong mineral acid solution to dissolve the Bi_2O_3.

2.3.3 Hydrothermal growth. This technique was used by Kolb et al. (1968) to grow rare earth and orthoferrite single crystals. They found that the quality of crystal was quite good with a few low angle grain boundaries.

Croxell et al. (1974) reported that by the hydrothermal growth method, they managed to grow crystals of zinc oxide using ultra-pure Zinc oxide powder.

They examined these crystals by using X-ray topography and found them to be of a high perfection - the principal imperfection being dislocations.

Most of hydrothermal growth is directed at growth of quartz for oscillators. Hosaka and Taki (1981) state that the best conditions to grow quartz crystals are: growth temperature above 400^{o}C and 10wt% KCl solution. Lias et al. (1973) reported that high quality quartz is grown by this method.

CHAPTER THREE

X-RAY DIFFRACTION TOPOGRAPHY

3.1 Introduction

X-ray diffraction topography refers to several diffraction techniques by which topographical displays of the microstructural defects in crystals can be obtained. It is concerned with the change in the intensity of the diffracted beams which have been diffracted by deformed regions which differ from the perfect crystal, that is because around the deformed region the Bragg condition breaks down, resulting in changes in the intensity of the diffracted beam (Tanner 1976). The Bragg condition is

$$n\lambda = 2d \sin\phi_B \qquad 3.1$$

λ is the radiation wave length and ϕ_B is the angle between incident beam direction and lattice planes.

X-ray topography is very similar to electron microscopy. The main difference between these two is that the X-ray technique is more sensitive to strain than electron microscopy and this is due to the much weaker scattering of X-rays by the crystal compared with electron microscopy. Because of the wide images in X-ray topographs, several micrometers wide, very low dislocation density crystals are required to reveal individual dislocations by this technique (Tanner 1977b).

Another difference is that multiple X-ray topographs may be taken of organic crystals. This would not be possible with the electron microscope, as the crystals would quickly volatalise or decompose (Lang 1978).

A list of all the X-ray topography techniques are covered by the first book on this subject (1976) and review articles

(1977a) of Tanner.

3.2 Orientation contrast and extinction contrast

Changes in the direction of the diffracted beam from point to point on the image is called orientation contrast (Lang 1978).

This contrast can be interpreted by simple geometry without using dynamical theory.

Extinction contrast arises from the distortion around the defect giving rise to different scattering power from those in the surrounding matrix (Tanner 1976). This is interpreted only by dynamical theory.

3.3 The dynamical Theory of X-ray diffraction

This theory was reviewed mathematically by Batterman (1964), also it is reviewed by Balchin and Whitehouse (1971).

There are two basic theories for the diffraction of X-rays by crystals, kinematical theory and dynamical theory. The main assumption of the former is that the amplitude of the diffracted beam is small compared with the incident beam amplitude. This works for small crystals but with large crystals the amplitude of the diffracted beam becomes comparable with that of the incident beam. The interaction between the diffracted and incident beam is however, taken into account by the latter theory (Tanner 1977b).

The problem, (Tanner 1977) is to solve Maxwell's equations in a periodic medium. The solution

$$\underline{D} = \exp iwt \; \Sigma \; \underline{D}_g \exp(-2\pi i \underline{k}_g . \underline{r}) \qquad 3.2$$

satisfies and the wave vectors $\underline{k}_g$ are linked by the Laue equation

$$\underline{k}_g = \underline{k}_o + \underline{g} \qquad 3.3$$

We see that the solution $\underline{D}$ inside the crystal consists of

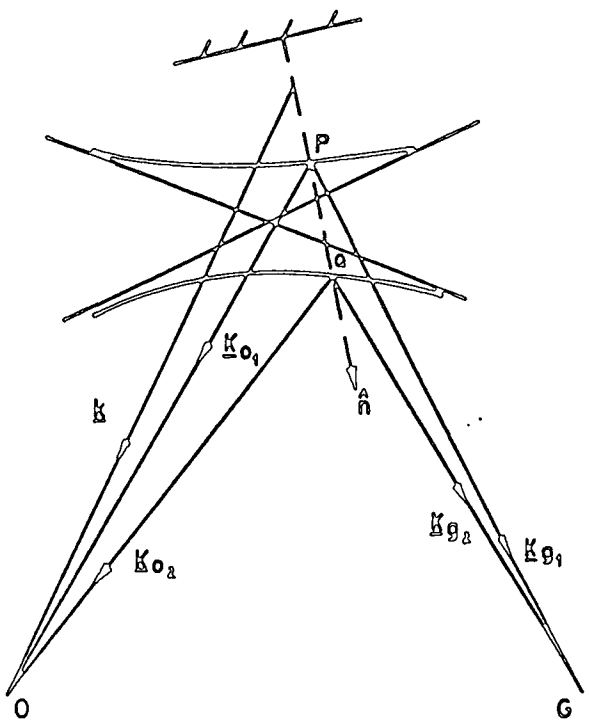

Figure 3.1 The dispersion surface construction (after Tanner 1977b).

a superposition of plane waves corresponding to a diffracted wave. This superposition is a wave field. In the X-ray case we need to consider two waves that are associated with the incident wave and that are associated with the diffracted wave. Neglecting time dependence we have wavefield of the form

$$\underline{D} = \underline{D}_o \exp(-2\pi i\, \underline{k}_o.\underline{r}) + \underline{D}_g \exp(-2\pi i\, \underline{k}_g.\underline{f}) \qquad 3.4$$

Substitution of this equation into a Maxwell's equation and the requirement for a non-trivial solution gives the relation between $\underline{k}_g$ and $\underline{k}_o$ and the amplitude ratio $R = \underline{D}_g/\underline{D}_o$ in terms of $\underline{k}_g$ and $\underline{k}_o$. The relation between $\underline{k}_g$ and $\underline{k}_o$ can be plotted graphically, and is known as the dispersion surface.

Close to the Bragg reflection the crystal potential raises the degeneracy, and there are four branches, two for each polarization state. Each point (tie point) on the dispersion surface (fig. 3.1) defines the wave vector and the wave amplitude inside the crystal. However, a single incident wave excites two Bloch waves and their associated wave vectors differ, and they interfere, giving rise to Pendellosung fringes. The depth period is known as the extinction distance ζ_g. For the symmetric Laue geometry

$$\zeta_g = \Lambda_o^{-1} = \pi V_c \cos\phi_B / r_e \lambda C (F_g F_{-})^{\frac{1}{2}} \qquad 3.5$$

where Λ_o is the diameter of dispersion surface and

V_c volume of unit cell

r_e classical electron radius

C Polarization factor

and F_g structure factor.

These fringes are important in the identification of high perfection crystals.

3.4 Experimental techniques

There are three techniques used with conventional X-ray generators.

(1) Berg-Barrett technique.

(2) Lang's technique.

(3) Double crystal technique.

3.4.1 Berg Barrett technque.

Figure (3.2a) shows the experimental arrangement.

The specimen, usually in the form of single crystal, is set to diffract the characteristic radiation from a chosen set of lattice planes using an extended source. Although a double image of any defect occurs because of the closely spaced $K\alpha_1$, $K\alpha_2$ doublet this is eliminated by placing the recording plate close to the specimen. In transmission, the overlapping of images from dislocations at different depths in the crystal limits the useful dislocation density to less than about 10^8 m^{-2} compared with about 10^{10} m^{-2} in reflection. Therefore surface reflection should be employed first for assessing a new crystal (Tanner 1976).

3.4.2 Lang's technique.

This is the most widespread topographic technique. In the Lang technique, commonly referred to as Lang topography, the crystal is usually studied in transmission rather than in back reflection. The essential features are shown in Figure (3.2b).

In this technique, if the crystal and film are stationary, the transmitted beam recorded in the photographic emulsion represents a small part of the crystal. This topograph is called a section topograph (Lang 1958).

If the crystal and film are both mounted on an accurate linear traversing mechanism, the whole area will then be recorded and the photograph obtained is called a projection topograph (Lang 1959). He also showed that a projection topograph is equivalent to a superposition of many section topographs.

A special method of projection topography was developed by Lang (1963) to record images only from those imperfections which are located within a selected range of depth in the crystal studied. The advantage of the "limited projection topograph" is that it disregards irrelevant surface damage, thus permitting study of the internal imperfections. This may be desired when surface damage is impossible or undesirable to remove. Double images rising from $K\alpha_1$ and $K\alpha_2$ are avoided by collimating the beam. Only $K\alpha_1$ is used due to its greater intensity (Tanner 1976).

3.4.3 Double-crystal technique

In this technique, originally due to Bond and Andrus (1952), the reference crystal and the specimen crystal have the same spacing of reflecting planes because the two crystals are from the same material, Figure (3.2c).

In this high sensitivity (+ -) parallel setting X-rays are diffracted from (hkl) and then from $(\bar{h}\bar{k}\bar{l})$. In this arrangement the diffraction from the specimen crystal will not occur unless the lattice planes of the reference and specimen crystal are nearly parallel. Thus this technique is very sensitive to the lattice distortion or misorientation.

When one of the crystals is rotated the rocking curve obtained is very narrow - typically a few seconds of arc,

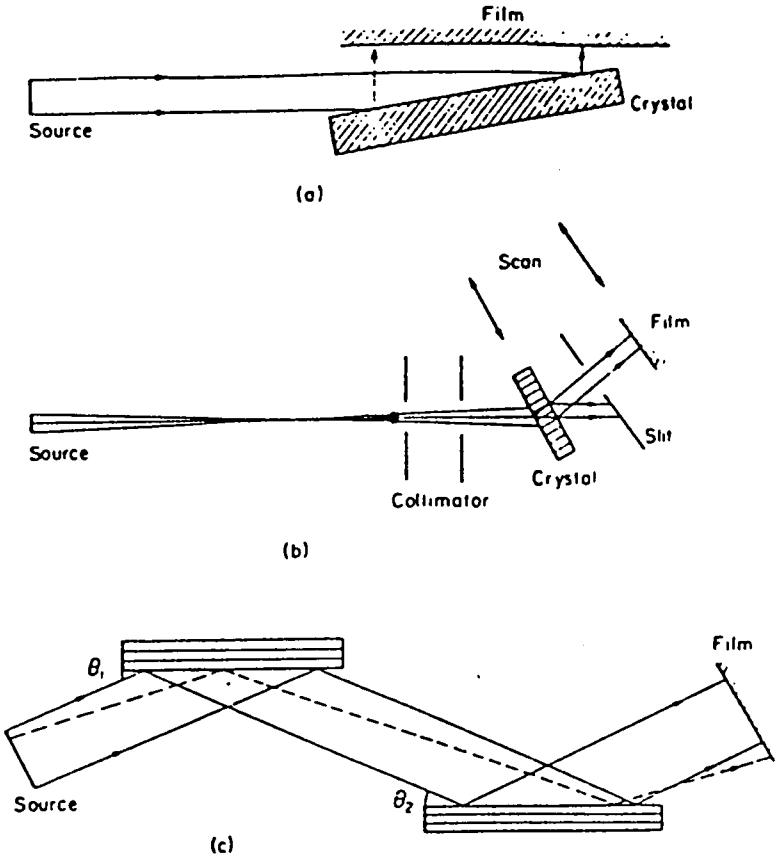

Figure 3.2 (a) The Berg-Barret technique.
(b) The Lang transmission technique.
(c) The double crystal technique (after Tanner 1977a).

if the misorientation is more than this, no diffracted intensity will reach the plate (Tanner 1977).

3.5 X-ray topography using synchrotron radiation.

Synchrotron radiation is electromagnetic radiation emitted when an electron is constrained to a circular orbit in a synchrotron or storage ring due to the central acceleration, which in the highly relativistic limit is seen in the laboratory frame as a narrow cone tangential to the electron orbit, whose angular divergence (ϕ) is given by

$$\phi \approx m_o c^2/E \qquad 3.6$$

where E is the electron energy and m_o is the rest mass. At Daresbury Laboratory the angular divergence is 10^{-4} radian (Tanner 1977a).

Because the radiation is a continuous spectrum extending through the visible and ultraviolet into the X-ray region the synchrotron beam is incident on a crystal and each crystal plane selects its own wavelength to satisfy the Bragg condition. A pattern of Laue spots is obtained which is easy to combine with another topographic experiment. Also there is no need for critical adjustments which is an advantage over the Lang technique. The other advantage is the great reduction in exposure time compared with laboratory sources, due to the very high intensity of the radiation which was the major complaint about X-ray topography. A further advantage is that the distance between the specimen and the plate can be increased without catastrophic loss of resolution. This enables the researcher to place his equipment around the specimen such as a magnetic field for studying magnetic domain motion step by step when the exposure time is in the order of seconds (Tanner 1977b).

The main disadvantage is the scarcity of synchrotron radiation laboratories.

3.6 Contrast of dislocation

There are three different types of image which have been classified by Authier (1978), namely direct image, intermediary image and dynamical image, Figure (3.3).

The dislocation line cuts the beam at P. Since the X-ray source is polychromatic, some of the X-rays which are not diffracted by a perfect crystal will be diffracted by the strained region around the dislocation. They thus suffer no primary extinction and appear as a dark spot with respect to the background of the plate. This is called the direct image. The dynamical image arises when the two wave fields decouple into their components as they cross the dislocation line at Q. They meet new wave-fields travelling in a new direction QL as they re-enter a perfect material. In the direction QL there is a loss of intensity and the dislocation line casts a light shadow with respect to the background of the plate and it is called the dynamical image. The intermediary image arises when the new wavefields interfere with the original wavefield and this type of image shows an oscillatory contrast (Tanner 1976).

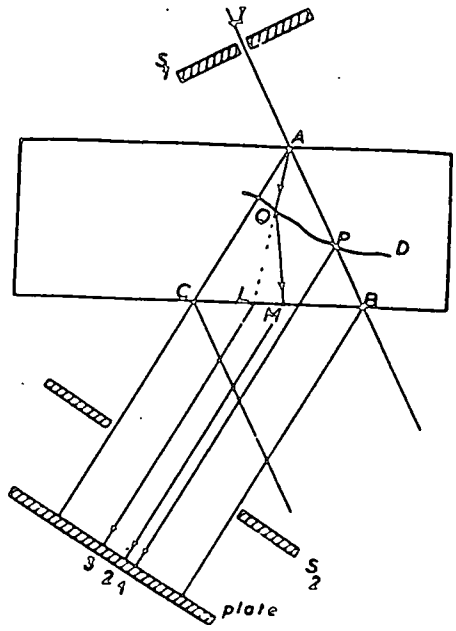

Figure 3.3 Formation of dislocation images in section and projection topographs.

1, Direct image,

2, Intermediary image,

3, Dynamical image (after Auther, A. 1978).

CHAPTER FOUR

SOME APPLICATIONS OF X-RAY TOPOGRAPHIC TECHNIQUES

4.1 Introduction

X-ray topography techniques are able to reveal the defects in crystal, thus by these methods one is able to determine the quality of crystals.

A useful review of the application of these techniques has been edited by Tanner and Bowen (1980).

This kind of technique helps crystal growth research to determine the best conditions for optimising the perfection of the crystal. It also enables research to study for example magnetic domain movement in situ or to compare their product with natural crystals, Lang (1978).

4.2 Berg-Barrett technique

Merz (1960) used a Berg-Barrett surface reflection topograph to see the change of the domain configuration in a cobalt zinc ferrite after applying a magnetic field.

Newkirk (1958) showed that by this technique dislocations in the polished surface of silicon crystals could be resolved.

Also Schultz and Armstrong (1964) used this technique to study zinc crystal grown from the melt. The topographs showed dislocation boundaries which are not resolved into individual lines.

Single crystals of beryllium oxide BeO which were grown from the flux have been studied by Austermann et al. (1965) using an X-ray diffraction topography. Twin boundaries are observed using this technique. Annealing treatment removed the damage caused by handling.

In single crystal of metals such as aluminium, zinc and copper, dislocations were observed using this technique

by Turner et al. (1968).

This method was used by Pielaszek (1975) to study the dislocation structure of nickel single crystal before and after electrolytic saturation with hydrogen. This technique was used by Frics (1981), as it gives information on the dislocation arrangement in a single crystal with a high dislocation, in the study of deformed single crystals as α - AL_2O_3, $(AL_2O_3)_{1.8}$ MgO, NaCl and Cu_2O.

4.3 Double crystal technique

X-ray double crystal topography was used by Baker and Hart (1976) to confirm that the sample of a gallium arsenide was dislocation free and they also observed that the internal strains were small.

Low angle grain boundaries was observed by Bye (1979) within cadmium mercury telluride crystal by using a double crystal reflection topograph.

.6 mm specimens of lithium fluoride crystal have been studied by Kohara (1970) using double crystal technique. The topographs show that the crystal consists of subgrains. Silicon web crystal doped with phosphor was also studied and dislocation lines were observed. Also annealed silicon crystals showed stacking faults.

Asymmetric double crystal topography technique is described by Boettinger et al. (1976) using copper, zinc and nickel sample crystals. They were able to observe subgrain boundaries and strains in zinc crystals. Magnetic domains in nickel crystal was observed.

Local strain in single crystal of BeO was determined by Chikawa (1967) using a double crystal arrangement. Synchrotron radiation double crystal X-ray topography was used

by Branett (1985) to examine 2 in. and 3 in. slices of GaAs in order to measure the lattice tilt and lattice parameter. They state that macroscopic structural inhomogeneity is due to lattice tilt fluctuations.

It was used by Jones (1981) to show a dislocation image and stacking faults in InP crystal grown by Czochralski method.

4.4 Lang's technique

Nost and Sorensen (1966) observed direct changes in dislocation densities in single crystals of aluminium during annealing treatment up to 400^{o}C by building a simple resistance furnace into a Lang Camera.

Lang and Polcarova (1965) studied thin plates cut from melt grown of iron silicon alloy single crystals which were then annealed and polished electrolytically and studied by Lang's technique. The topograph shows that the crystal is divided into a large subgrain in which the dislocation density is low.

Nes and Nost (1960) used Lang's technique to study the relation between dislocation density in strain anneal grown aluminium and the cooling rate. They found that the dislocation density was proportional to the cooling rate.

Thin oriented sections of Fe-Si single crystal were cut by electric spark method, then electropolished after they were annealed in dry hydrogen. Polcarova and Lang (1962) were able to observe magnetic domain configuration and their movements under the application of a magnetic field.

Single crystals of hexamethaline tetramine grown from ethanol solution were examined using Lang's technique by Duckett and Lang (1973). It was seen that these crystals

contained a low dislocation density and any Pendellosung fringes which were recorded indicated that those crystals were of high perfection.

Chikawa (1974) used a rotating Mo target X-ray generator, which is operated at 60 Kv, and a PbO vidicon camera tube which is fitted with a beryllium window to view Lang topographs directly. The system was applied to in situ observation of the melting and growth process in a silicon single crystal. He observed dislocation generation as the melting of the silicon crystal occurred.

It was used by Tanner and Smith (1975) to identify the perfection of crystals of $TbVO_4$ and $TmVO_4$ which were grown from $Pb_2V_2O_7$ flux by slow cooling. The topograph shows the quality of these crystals.

Dislocation lines in the crystals which were grown by slow cooling from flux were observed by Safa et al. (1977).

Patel (1973) used an X-ray section topograph to follow the perfection process of a silicon crystal, Parallel Pendellosung fringes indicate that the crystal is of high perfection after one hour at $1000^{o}C$. The Pendellosung fringes are still relatively clear and dark spots occur. After six hours at $1000^{o}C$ the Pendellosung fringes have disappeared and the spots appear to lie in bands.

Vale and Smallman (1977) prepared magnesium crystals to investigate oxidation behaviour by X-ray topography. They were able to see the growth of dislocation during their treatment. The topographs reveal the dislocation loops.

Dislocation helices in a single crystal of molybdenum produced by strain anneal technique were observed using Lang's

technique by Becker and Pegel (1969).

In (1969) Pegel and Becker state that by applying a small stress to this sample, the helices were removed from the specimen leaving pure screws in the crystal.

Lang's method was used by Rek (1972) to observe the formation of dislocations in silicon single crystals after applying a hydrostatic pressure.

The effect of oxide particles attached to the tin crystal was observed by Fiedler and Lang (1972). The dislocation extending at a rate of 1μm per hour over a period of weeks.

4.5 Synchrotron white beam technique

Tanner et al. (1977a) showed that images of dislocations taken of a thin polished specimen by synchrotron radiation looks similar to the image obtained by Lang's technique. Small cracked regions of crystal do not appear with Lang's technique but do appear with synchrotron radiation because the crystal selects different wavelengths from the white beam to diffract.

Domain wall movement in $KNiF_3$ and $KCoF_3$ grown from the flux at high temperature, was observed by Safa and Tanner (1978) using a magnetic field.

However, even though the exposure time is in the order of seconds in magnetic domain movement experiments, the time needed for changing the X-ray plate will increase the experiment time. Thus, the Durham group have built a simple cassette holding six plates. This can be controlled from outside and this will decrease the experiment time because there is no need to open the experiment area and close it again to change the X-ray plate (Tanner 1977a).

The first insitu experiment using synchrotron white beam topography to study crystal growth under normal growth conditions was done by MacCormack and Tanner (1978). They used a commercial silicon iron sheet rolled so the thickness was reduced by 85% to 370 micrometer. The sequence of micrographs showing the development of the grain growth during precrystallisation was recorded on polaroid film. Through this technique Jourdan and Gasteldi (1979) were able to follow step by step the boundary migration in aluminium single crystal during recrystallization.

It was also used by Tohano et al. (1985) to study in situ the dislocation behaviour for S-doped InP crystal during deformation at 450^{o}C.

Silicon Carbide (SiC) specimens, which are generally very distorted crystals that cannot be examined by Lang's technique, were investigated by Fisher and Barnes (1984) using white beam, and the crystal topograph revealed low angle boundary.

CHAPTER FIVE

A THEORETICAL STUDY OF TEMPERATURE DISTRIBUTION ON CRYSTALS GROWN BY CZOCHRALSKI TECHNIQUE

5.1 Introduction

This calculation of the temperature profile in the crystal is based on the model of Buckley-Golder and Humphreys (1979). It was done for four elements, silver, copper, silicon and nickel. The first three elements were reproduced because of the difference in calculation of the Biot number (Table 5.1) and in the calculation of C_5 (equation 2.10, Buckley-Golder 1977). The fourth one was because the work at Durham University was concerned with producing high quality nickel single crystals.

In order to produce crystals with low dislocation density the temperature gradient should be minimized. Thus, the crystal neck and seed size were varied to see how this would affect the temperature gradient of the crystal and to look for the best way to minimize the temperature gradient.

5.2 Formulation of the model

Following Buckley-Golder 1977, let us assume that a seed, neck and crystal are 'sitting' on a liquid (Figure 5.1), and let us also assume that the element in the liquid, seed, neck and crystal be the same throughout and that the exhibit is cylindrically symmetrical. It was taken that the crystal grows into a constant ambient temperature and the heat transfer process occurs:

(1) Conduction up the crystal.

(2) Radiation from surface such as A and B in Figure (5.1).

If the temperature distribution for any element Δz depends on z only, it is appropriate to apply the heat transfer equations for a cylindrical rod.

he heat transfer equation for a cylindrical rod is written as

$$c\rho A \frac{\partial T(z)}{\partial t} = KA \frac{\partial^2 T(z)}{\partial z^2} - h_R p \, (T(z) - T_A) \qquad 5.1$$

where c and p are the specific heat capacity and density, respectively, of the element considered.

A is the cross section area of rod

T(z) is the temperature of the rod at a given point z in Figure 5.1.

K is the thermal conductivity

h_R is the heat radiation coefficient

T_A is the ambient temperature

and p is the circumference of the rod.

In the time independent condition

$(\frac{\partial T(z)}{\partial t} = 0)$ equation (5.1) reduces to

$$\frac{d^2 T(z)}{dz^2} = n^2 \, [T(z) - T_A] \qquad 5.2$$

where $n^2 = \frac{h_R p}{KA} = \frac{h_R 2\pi R}{K\pi R^2} = \frac{2h_R}{KR} = \frac{2B_i}{R^2}$ 5.3

R is the radius of the rod and

$$B_i = \frac{h_R R}{K} \qquad 5.4$$

This equation was used by Buckley-Golder and Humphreys (1979) as $B_i = \frac{h^2 R}{K}$ which was an error in their calculation (Table 5.1)

B_i is the Biot number (it is a dimensionless quantity).

The solution of equation 5.2 is

$$T(z) = T_A + \cosh\left[\frac{(2B_i)^{\frac{1}{2}}}{R_i} z\right] C_1 + \sinh\left[\frac{(2B_i)^{\frac{1}{2}}}{R} z\right] C_2 \quad 5.5$$

where C_1 and C_2 are the integration constants

$$\text{Define } X_i = \frac{(2B_i)^{\frac{1}{2}}}{R_i} \quad 5.6$$

Assuming that the diameters of the seed, neck and crystal are constant through their length, then

$$T_C(z) = T_A + \cosh(X_C z)C_1 + \sinh(X_C z)C_2 \quad 5.7a$$

$$T_n(z) = T_A + \cosh(X_n z)C_3 + \sinh(X_n z)C_4 \quad 5.7b$$

$$T_s(z) = T_A + \cosh(X_s z)C_5 + \sinh(X_s z)C_6 \quad 5.7c$$

where C, n and s refer to crystal neck and seed respectively. The constants C_1 to C_6 can be determined by the following six boundary conditions:-

$$z = 0 \qquad T_c(0) = T_m \quad 5.8a$$

$$z = L_C \qquad T_c(L_c) = T_n(L_c) \quad 5.8b$$

$$z = L_n \qquad T_n(L_n) = T_s(L_n) \quad 5.8c$$

$$z = L_s \qquad T_s(L_s) = T_A \quad 5.8d$$

$$kA_c \frac{dT_c(L_c)}{dz} = kA_n \frac{dT_n(L_c)}{dz} + h_{Rc}(A_c - A_n)\,[T_c(L_c) - T_A] \quad 5.8e$$

$$kA_n \frac{dT_n(L_n)}{dz} = kA_s \frac{dT_s(L_n)}{dz} + h_{Rs}(A_s - A_n)\,[T_n(L_n) - T_A] \quad 5.8f$$

Thus, the temperature T(z) is defined at all points as the temperature gradient by differentiating equations 5.7a, 5.7b and 5.7c.

$$\frac{dT_c(L_c)}{dz} = X_c \sinh(X_c L_c)C_1 + X_c \cosh(X_c L_c)C_2 \quad 5.9a$$

$$\frac{dT_n(L_n)}{dz} = X_n \sinh(X_n L_n)C_3 + X_n \cosh(X_n L_n)C_4 \quad 5.9b$$

$$\frac{dT_s(L_s)}{dz} = X_s \sinh(X_s L_s) C_5 + X_s \cosh(X_s L_s) C_6 \qquad 5.9c$$

5.3 The solution of the equations for the constants C_1 to C_6

Applying the condition 5.8a to the equation 5.7a we obtain

$$C_1 = T_m + T_A \qquad 5.10I$$

Define $S_{ij} = \sinh(X_i L_j)$

using equations 5.7a and 5.7b with the condition 5.8b, equation 5.7b and 5.7c with the equations 5.8c we find

$$C_{cc}C_1 + S_{cc}C_2 - C_{nc}C_3 - S_{nc}C_4 = 0 \qquad 5.11$$

and

$$C_{nn}C_3 + S_{nn}C_4 - C_{sn}C_5 - S_{sn}C_6 = 0 \qquad 5.12$$

from equation 5.7c and the condition 5.8d we get

$$C_6 = \xi C_5 \qquad 5.10II$$

where

$$\xi = -\frac{C_{ss}}{S_{ss}} \qquad 5.13$$

From 5.7a, 5.8e, 5.9a and 5.9b, we obtain

$$[kA_cX_cC_{cc} - h_{Rc}(A_c - A_n)S_{cc}]C_2 - [kA_nX_nS_{nc}]C_3 - [kA_nX_nC_{nc}]C_4 = [h_{Rc}(A_c - A_n)\,C_{cc} - kA_cX_cS_{cc}]C_1 \qquad 5.14$$

from 5.7b, 5.8f, 5.9b and 5.9c, we find

$$[kA_nX_nS_{nn} - h_{Rs}(A_s - A_n)C_{nn}]C_3 + [kA_nX_nC_{nn} - h_{Rs}(A_s - A_n)S_{nn}]C_4 = kA_sX_s\,(S_{sn} + \xi C_{sn})]C_5 \qquad 5.15$$

It follows from equation 5.11 that

$$C_2 = [C_{nc}C_3 + S_{nc}C_4 - C_{cc}C_1]/S_{cc} \qquad 5.10III$$

From equation 5.12, we get

$$C_5 = [C_{nn}C_3 + S_{nn}C_4] \;/\; [C_{sn} + \xi S_{sn}] \qquad 5.10iv$$

Substituting equation 5.10III into equation 5.14, we obtain

$$\alpha_1[C_{nc}C_3 + S_{nc}C_4 - C_{cc}C_1] - \alpha_2C_3 - \alpha_3C_4 = \alpha_4 \quad 5.16$$

where $\alpha_1 = (kA_cX_cC_{cc}/S_{cc}) - [h_{Rc}(A_c - A_n)]$ 5.17

$$\alpha_2 = kA_nX_nS_{nc} \quad 5.18$$

$$\alpha_3 = kA_nX_nC_{nc} \quad 5.19$$

and

$$\alpha_4 = [h_{Rc}(A_c - A_n)C_{cc} - kA_cX_cS_{cc}]C_1 \quad 5.20$$

Substituting equation 5.10IV into equation 5.15, we find

$$B_1C_3 + B_2C_4 - B_3(C_{nn}C_3 + S_{nn}C_4) = 0 \quad 5.21$$

where

$$B_1 = kA_nX_nS_{nn} - h_{Rs}(A_s - A_n)C_{nn} \quad 5.22$$

$$B_2 = kA_nX_nC_{nn} - h_{Rs}(A_s - A_n)S_{nn} \quad 5.23$$

and

$$B_3 = kA_sX_s(S_{sn} + \xi C_{sn})/(C_{sn} + \xi S_{sn}) \quad 5.24$$

Equation 5.16 and 5.21 can be rewritten as

$$C_3[\alpha_1C_{nc} - \alpha_2] + C_4[\alpha_1S_{nc} - \alpha_3] = \alpha_4 + \alpha_1C_{cc}C_1 \quad 5.25$$

$$C_3[B_1 - C_{nn}B_3] + C_4[B_2 - S_{nn}B_3] = 0 \quad 5.26$$

It follows from equation 5.26 that

$$C_3 = \gamma C_4 \quad 5.10V$$

where

$$\gamma = -[B_2 - S_{nn}B_3] / [B_1 - C_{nn}B_3] \quad 5.27$$

Substituting equation 5.10V into equation 5.25 we finally obtain

$$C_4 = (\alpha_4 + \alpha_1C_{cc}C_1)/[\gamma(\alpha_1C_{nc} - \alpha_2) + \alpha_1S_{nc} - \alpha_3] \quad 5.10IV$$

This constant was calculated by a computer programme (see Appendix A).

5.4 Results

These results were obtained when the radiation losses were high.

5.4.1 Varying the seed length and radius

From figure 5.2 and Table 5.3 it can be seen that reducing the seed length from 60 to 20 mm had a minimal effect on the temperature gradient of the crystal. Also as in Figure 5.3 and Table 5.4 it is clear that reducing seed radius from 3 to 1.5 mm has no obvious affect on the temperature gradient on the crystal.

5.4.2 Varying the neck length

It is clear from Table 5.5 and Figure 5.4 that increasing the neck length from 2 to 4 and finally to 8 mm, will reduce the temperature gradient noticeably in copper and silver, whilst in silicon and nickel the effect is minimal.

5.4.3 Varying the neck radius

Increasing neck radius from .1 to .2 and finally to .4 mm increases the temperature gradient in all these four elements (Table 5.6 and Figure 5.5).

5.4.4 Varying the crystal length

From Figure 5.6 and Table 5.7 the crystal length has a noticeable effect on the temperature gradient of the crystal. As the crystal length increases the temperature gradient increases markedly in these elements.

5.4.5 Varying the crystal radius

Increasing crystal radius from 1 to 2 mm decreases the temperature gradient in the crystal, and decreasing crystal radius from 1 to 0.5 mm increased the temperature

gradient of the crystal, as is clear from Figure 5.7 and Table 5.8.

5.4.6 A comparison between the four elements

Tables 5.9, 5.10, and Figures 5.8, and 5.9, represent the changes in temperature gradient of the crystal at z = 0 caused by varying the neck radius and length respectively for Ag, Cu, Ni and Si.

In Figure 5.9 as the neck radius increases the temperature gradient increases for all these elements. In Figure 5.10 the change in temperature gradient is very small in Ni and Si compared with the change in Ag and Cu.

Tables 5.11 and 5.12 and Figures 5.10 and 5.11 represent the change in temperature gradient of the crystal at z = 0 caused by varying the crystal radius and length respectively.

5.4.7 A study of the effect of Ni crystal radius

The effect of varying the crystal radius of Ni crystal with 6 and 10 mm length is shown in Table 5.13 and Figure 5.12. The neck radius and length were 0.1 and 2 mm respectively, with the seed radius and length 3 and 60 mm respectively. A lower value for temperature gradient on the crystal was obtained with small crystal length and large diameter.

5.5 Conclusion

The seed length and radius has a minimal effect on the temperature gradient on the crystal for these four elements.

Neck radius has a great effect in reducing the temperature gradient. Neck length has an obvious effect on copper and silver but not in silicon or nickel.

As crystal radius is increased the temperature gradient is reduced whilst the temperature gradient increases as the crystal length is increased.

The data collected leads us to a conclusion similar to that of Buckley-Golder and Humphreys (1979). This is that the crystal grown should be short and fat with a long and thin neck. The seed should preferably be long and thin in order to reduce the temperature gradient of the crystal.

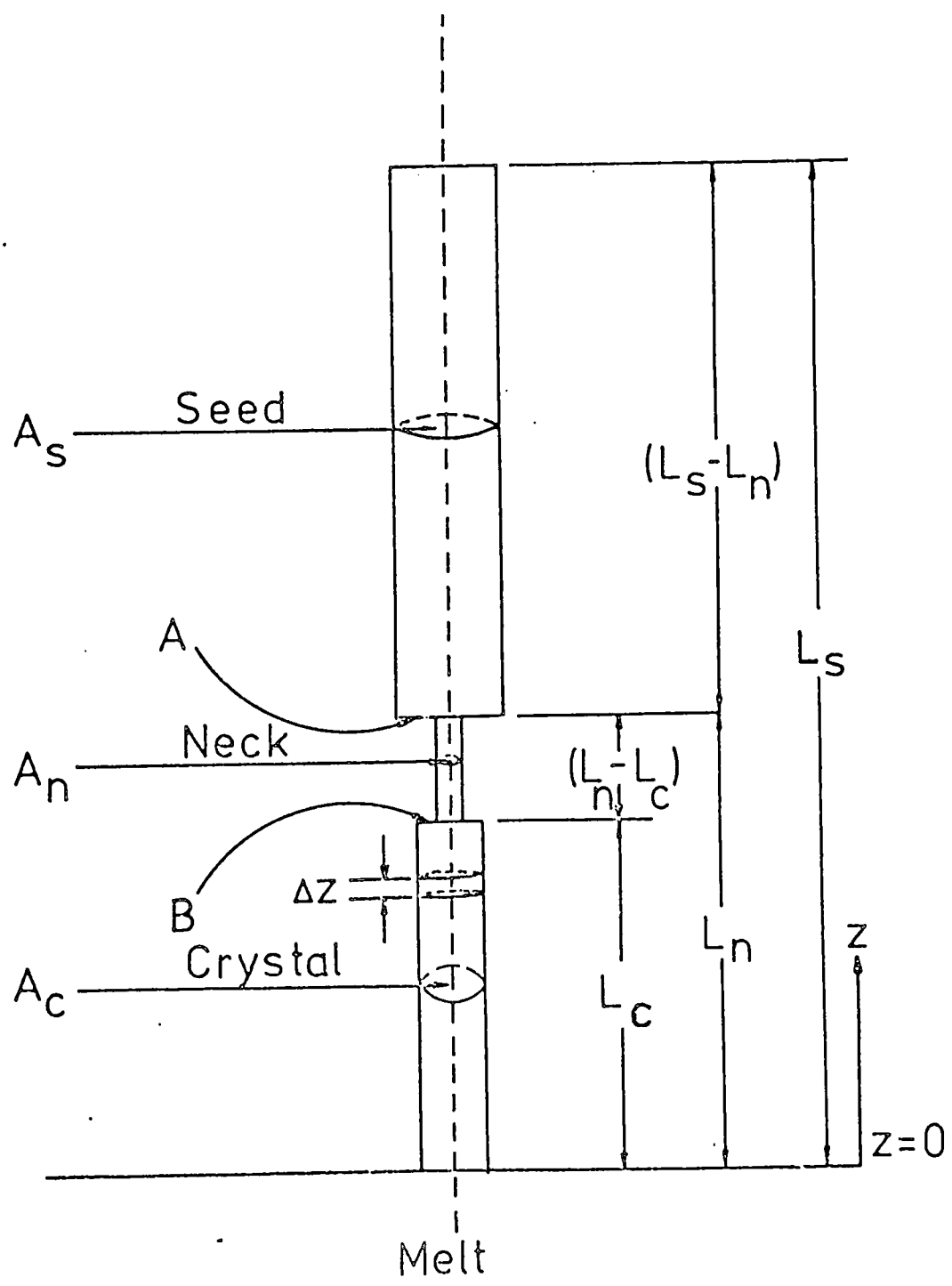

Figure 5.1 The crystal growth model. A_c, A_n and A_s are the cross-sectional areas of the crystal, neck and seed, respectively. L_c, (L_n-L_c) and (L_s-L_n) are the lengths of the crystal, neck and seed, respectively. (Buckley-Golder and Humphreys, 1979).

TABLE 5.1

Previous calculation of copper $B_i = h_R R^2/K$		Present calculation $B_i = h_R R/K$
1.47×19^{-4}	(crystal)	1.47×10^{-4}
3.30×10^{-6}	(neck)	2.219×10^{-5}
1.32×10^{-3}	(seed)	4.429×10^{-4}
Previous calculation of silicon		**Present calculation**
2.05×10^{-3}	(crystal)	2.067×10^{-3}
4.61×10^{-5}	(neck)	3.107×10^{-4}
1.84×10^{-2}	(seed)	6.201×10^{-3}

TABLE 5.2

The Basic Parameters used in this calculation

element	k (w/mm/k)	Tm (c)	TA (c)	E at 0.65μm	radius mm		length mm	Area mm^2	B_i X1.4 low radiation	B_i high radiation
cu	0.342	1083.0	983.0	0.10	crystal	1	3	3.1415	1.479×10^{-4}	2.07×10^{-4}
					neck	.1	2	3.145×10^{-2}	1.479×10^{-5}	2.07×10^{-5}
					seed	3	60	28.274	4.439×10^{-4}	6.21×10^{-4}
Si	2.51×10^{-2}	1410.0	1279.0	0.46	crystal	1	3	3.1415	1.762×10^{-2}	2.467×10^{-2}
					neck	.1	2	3.145×10^{-2}	1.76×10^{-3}	2.467×10^{-3}
					seed	3	60	28.274	5.28×10^{-2}	7.40×10^{-2}
Ni	5.899×10^{-2}	1453.0	1318.0	0.5041	crystal	1	3	3.145	8.856×10^{-3}	1.239×10^{-2}
					neck	.1	2	3.145×10^{-2}	8.856×10^{-4}	1.239×10^{-3}
					seed	3	60	28.274	2.656×10^{-2}	3.719×10^{-2}
Ag	0.363	961.9	872.0	7×10^{-2}	crystal	1	3	3.1415	9.381×10^{-5}	1.033×10^{-4}
					neck	.1	2	3.145×10^{-2}	7.381×10^{-6}	1.03×10^{-5}
					seed	3	60	28.274	2.214×10^{-4}	3.10×10^{-4}

TABLE 5.3

Reducing the seed length from 60 to 20 mm

element	seed length = 60 mm $DT_c(0)$	seed length = 20 mm $DT_c(0)$
cu	- 0.58417	- 0.59254
Si	- 15.45943	- 15.45945
Ni	- 8.72141	- 8.72158
Ag	- 0.47696	- 0.48529

TABLE 5.4

Reducing the seed radius from 3 to 1.5 mm

element	seed radius = 3 mm $DT_c(0)$	seed radius = 1.5 mm $DT_c(0)$
cu	- 0.58417	- 0.55291
Si	- 15.45943	- 15.45726
Ni	- 8.72141	- 8.71666
Ag	- 0.47696	- 0.44497

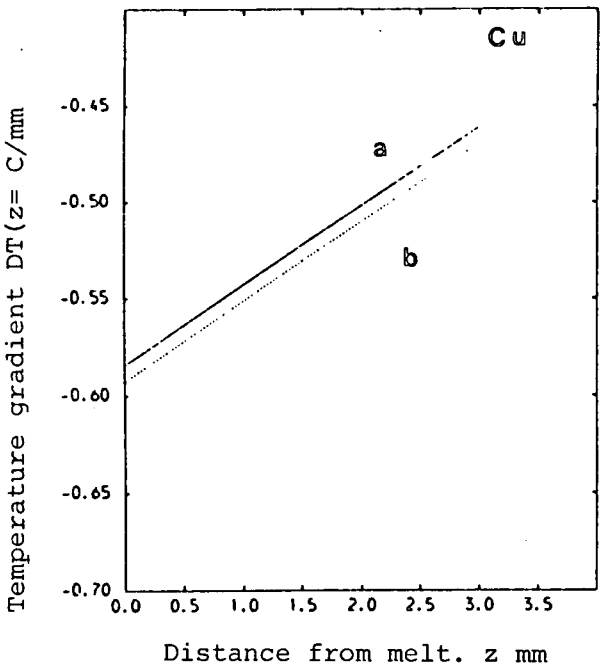

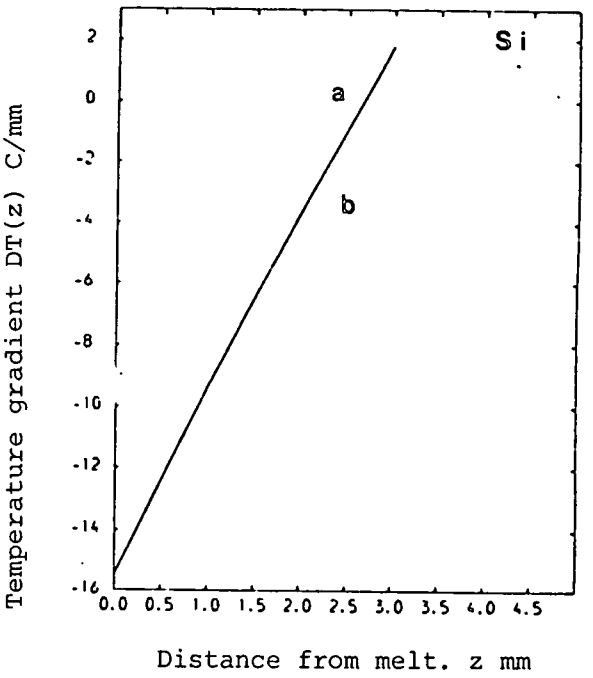

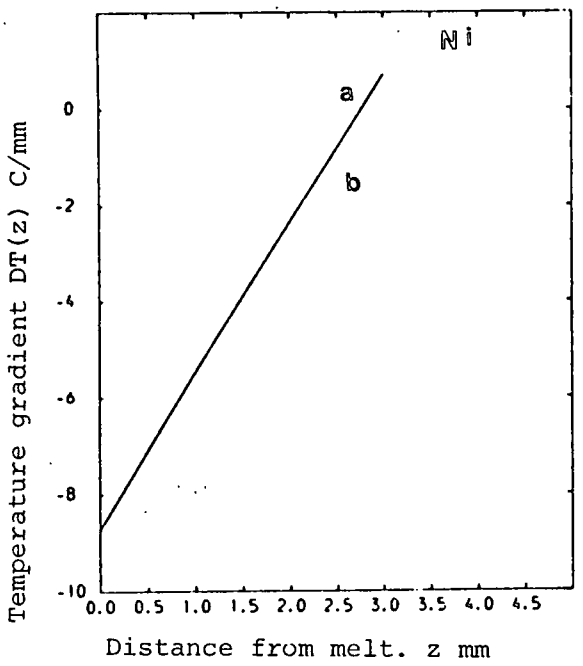

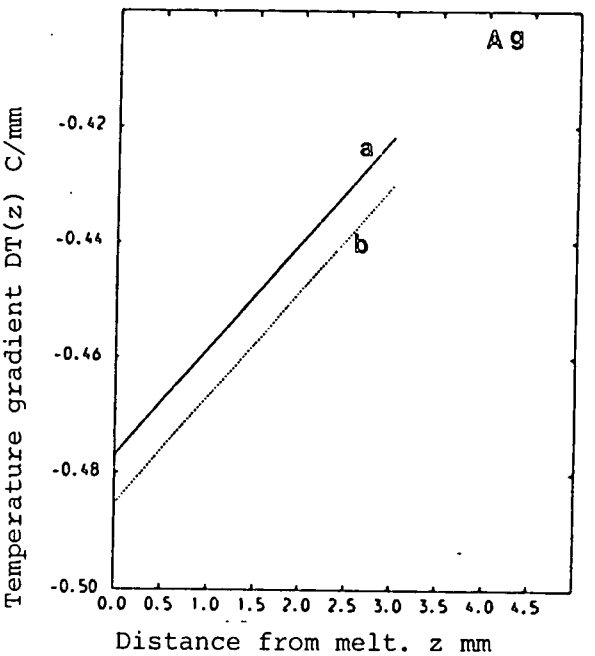

Figure 5.2 Reducing the seed length from 60 to 20 mm.

seed length a = 60 mm

b = 20 mm

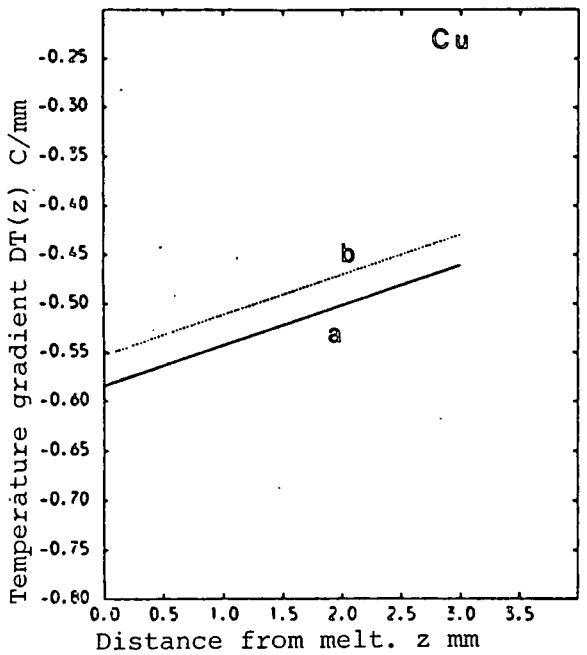

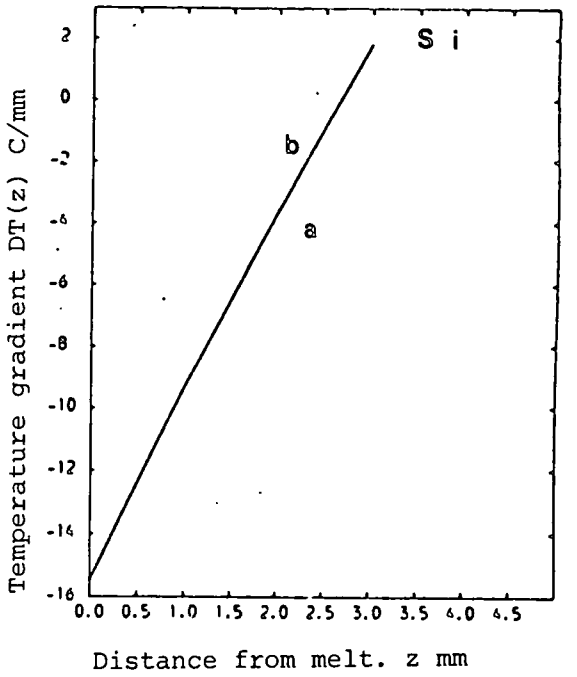

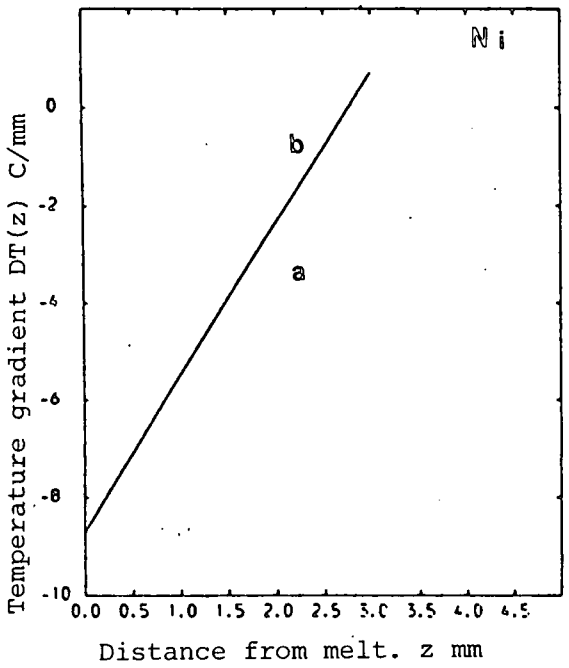

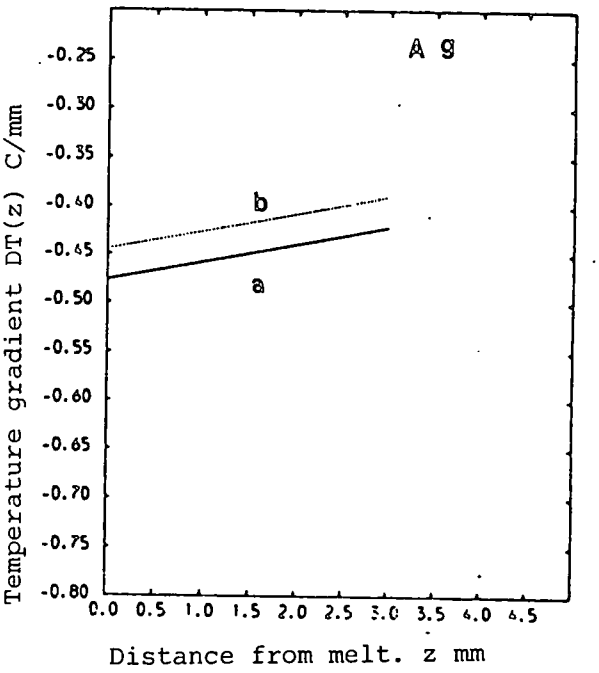

Figure 5.3 Reducing the seed radius from 3 to 1.5 mm

seed radius a = 3 mm

b = 1.5 mm

TABLE 5.5

Increasing the neck length

element	neck length = 2 mm $DT_c(0)$	neck length = 4 mm $DT_c(0)$	neck length = 8 mm $DT_c(0)$
cu	- 0.58417	- 0.35319	- 0.23786
Si	- 15.45943	- 15.38025	- 15.37549
Ni	- 8.72141	- 8.56771	- 8.54698
Ag	- 0.47696	- 0.26842	- 0.16239

TABLE 5.6

Increasing the neck radius

element	neck radius = 1 mm $DT_c(0)$	neck radius = .2 mm $DT_c(0)$	neck radius = .4 mm $DT_c(0)$
cu	- 0.58417	- 1.80609	- 4.79978
Si	- 15.45943	- 17.14211	- 21.86757
Ni	- 8.72141	- 10.50171	- 15.62846
Ag	- 0.47696	- 1.56598	- 4.19071

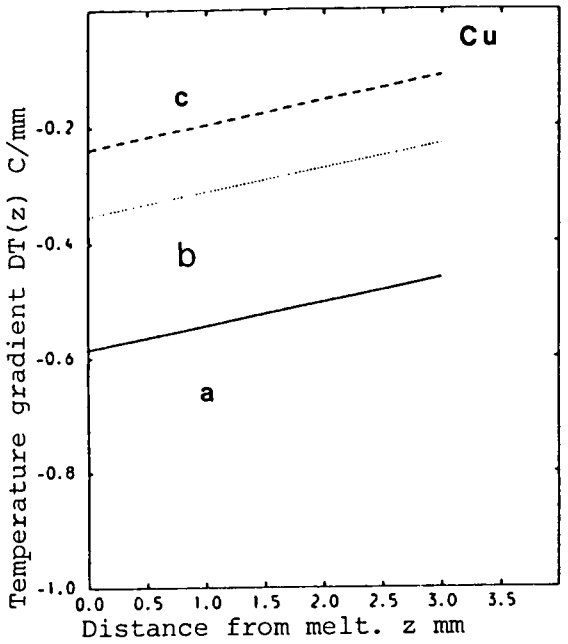

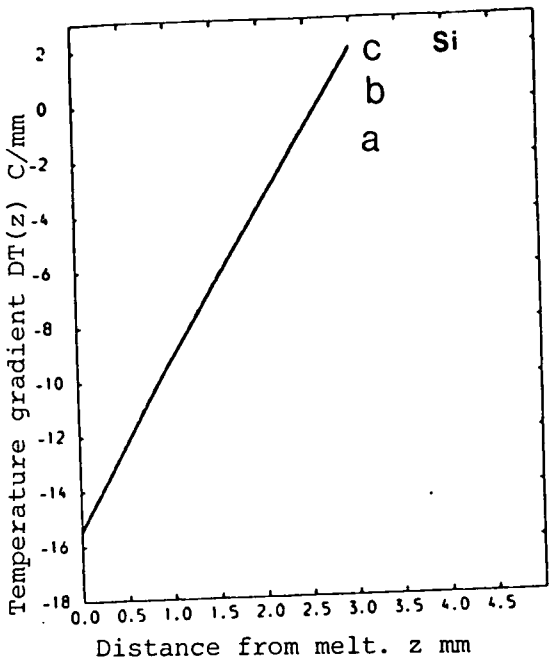

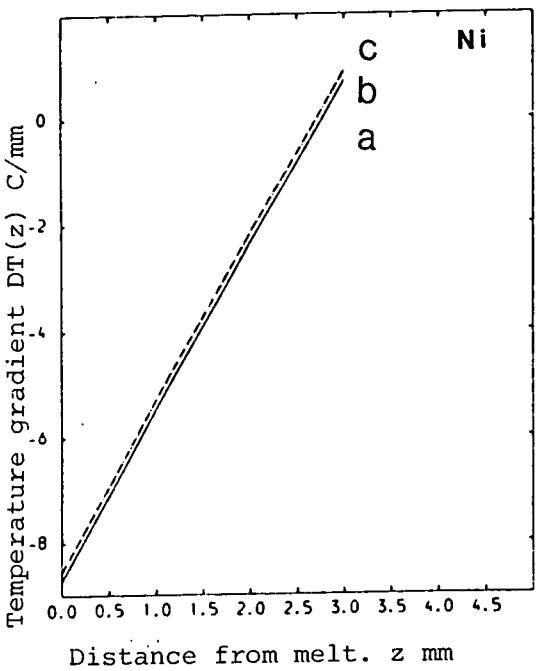

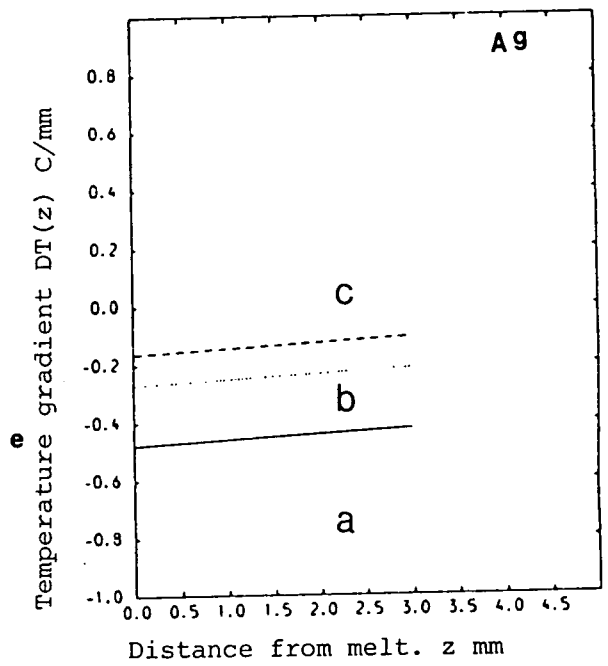

Figure 5.4 Increasing neck **length** from 2 to 4 and and finally to 8 mm

neck **length** a = 2 mm
b = 4 mm
c = 8 mm

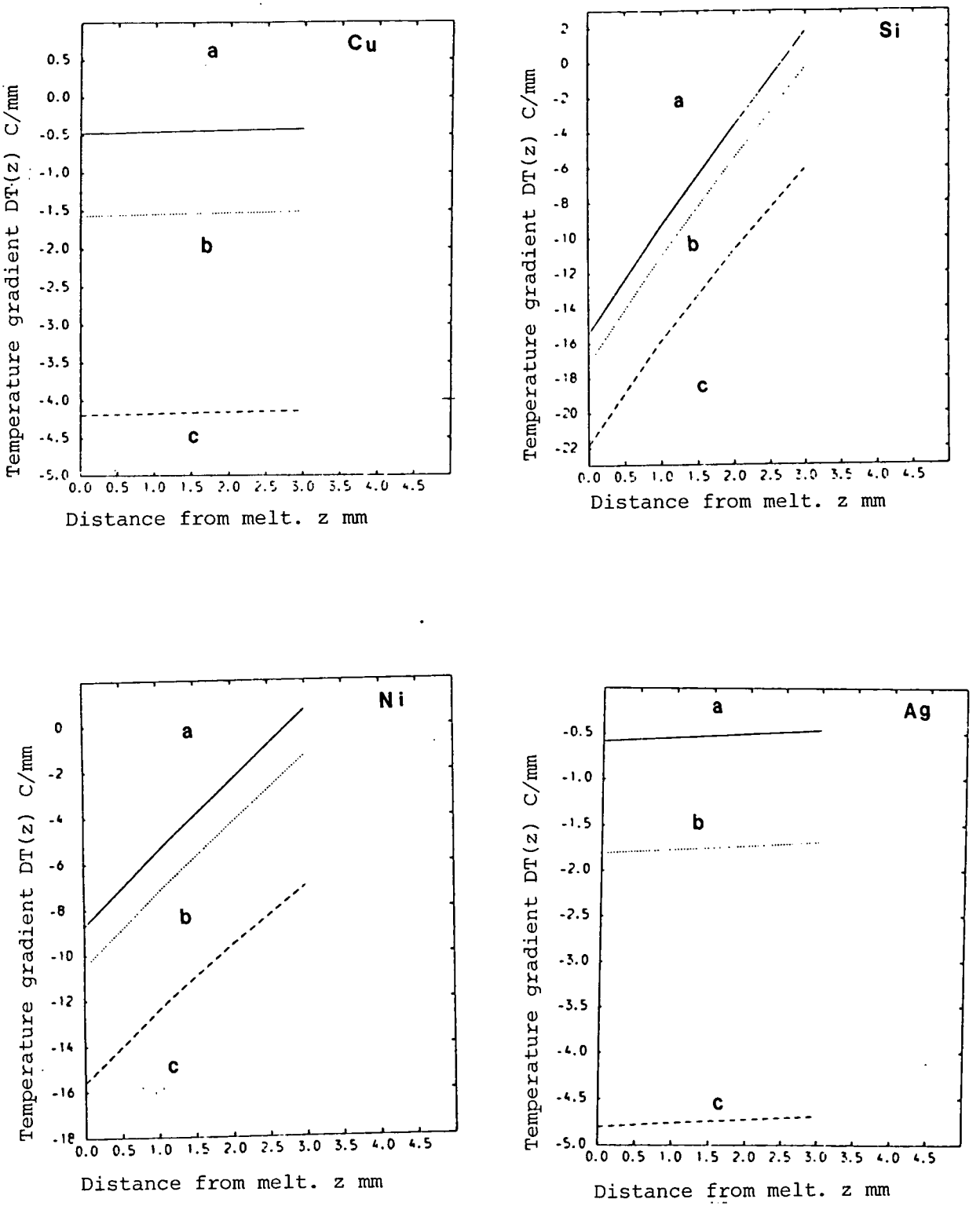

Figure 5.5 Increasing neck radius from .1 mm to .2 mm and finally to .4 mm

neck radius a = .1 mm
b = .2 mm
c = .4 mm

TABLE 5.7

Increasing the crystal length

element	crystal length = 3 mm $DT_c(0)$	crystal length = 6 mm $DT_c(0)$	crystal length = 12 mm $DT_c(0)$
cu	- 0.58417	- 0.69614	- 0.90586
Si	- 15.45943	- 24.75156	- 28.77459
Ni	- 8.72141	- 15.31342	- 20.23944
Ag	- 0.47696	- 0.52433	- 0.61411

TABLE 5.8

Increasing the crystal radius

element	crystal radius = 0.5 mm $DT_c(0)$	crystal radius = 1.0 mm $DT_c(0)$	crystal radius = 2 mm $DT_c(0)$
cu	- 2.06353	- 0.58417	- 0.16313
Si	- 30.770277	- 15.45943	- 6.48199
Ni	- 18.76881	- 8.72141	- 3.50219
Ag	- 1.74998	- 0.47696	- 0.12749

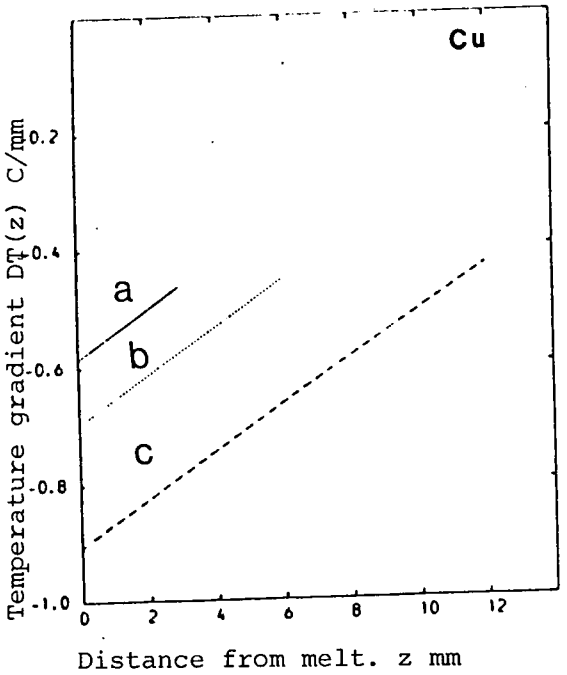

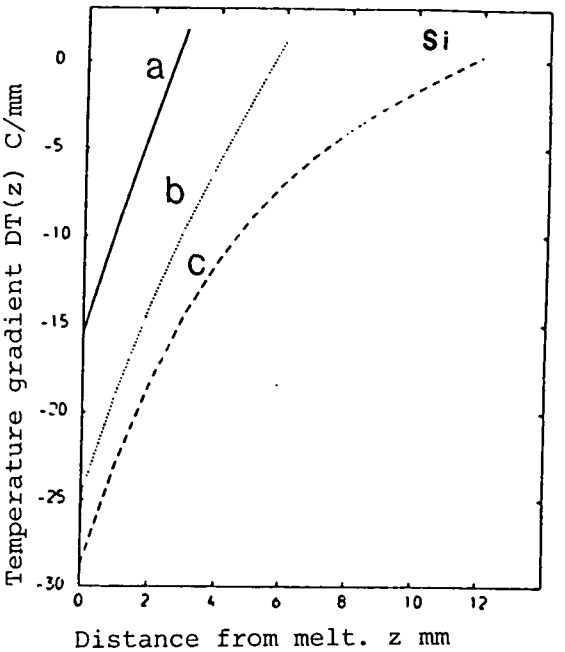

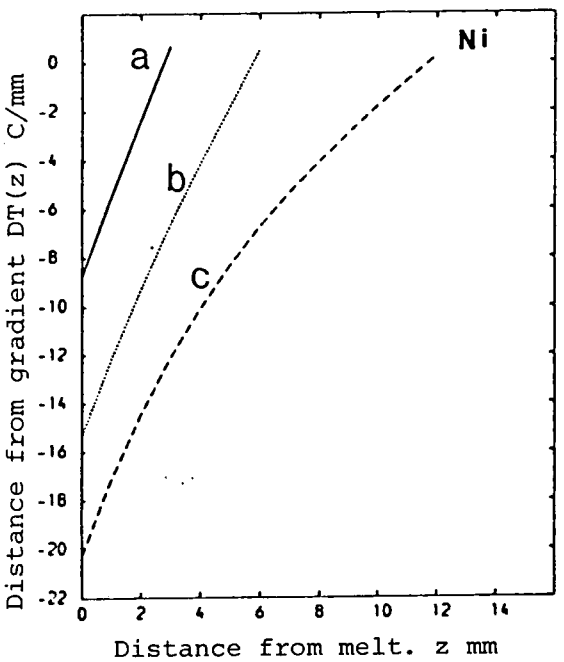

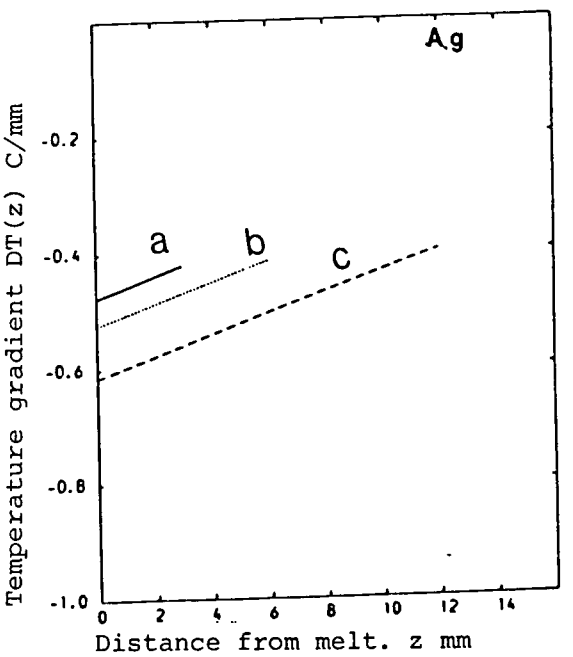

Figure 5.6 Increasing crystal length from 3 to 6 and finally to 12 mm

crystal length a = 3 mm
b = 6 mm
c = 12 mm

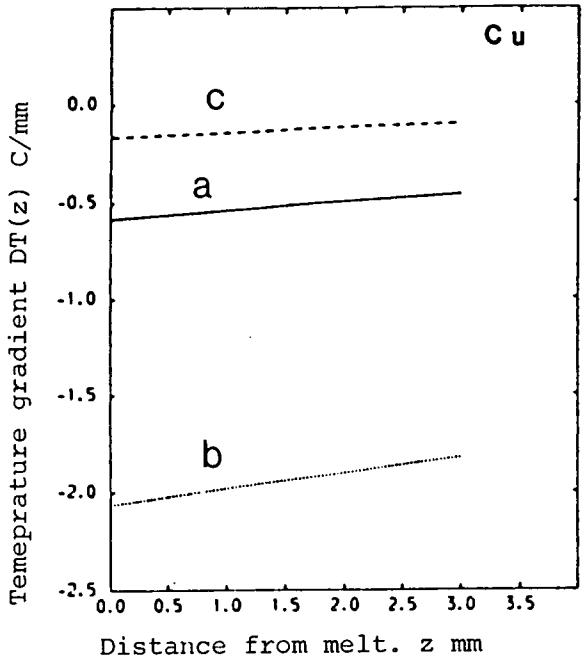

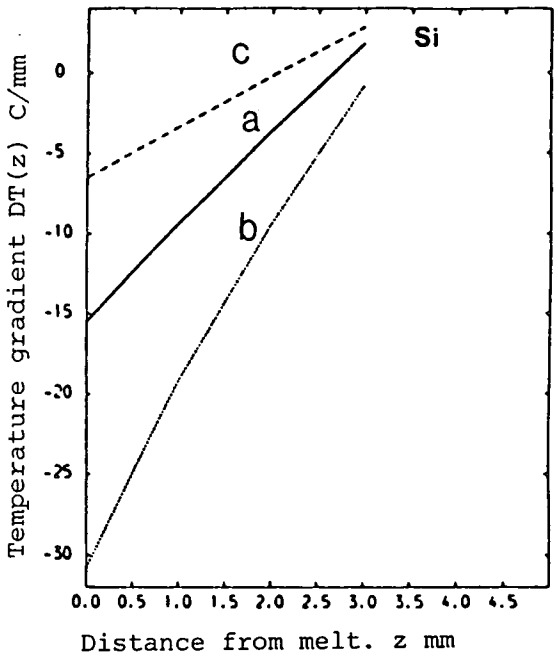

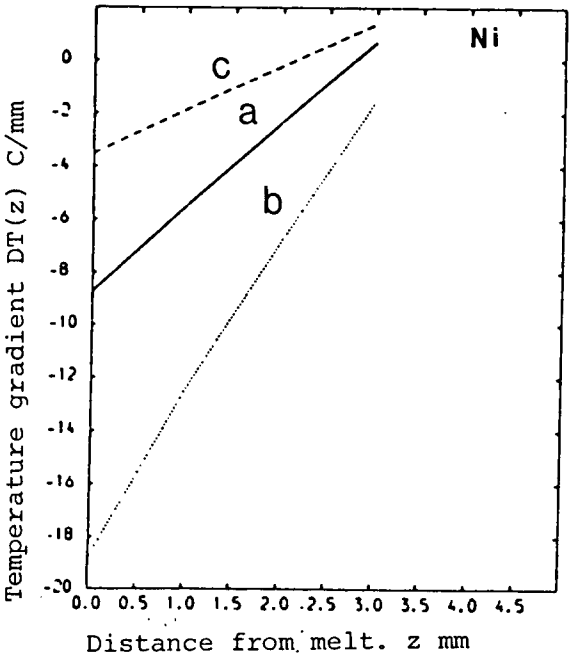

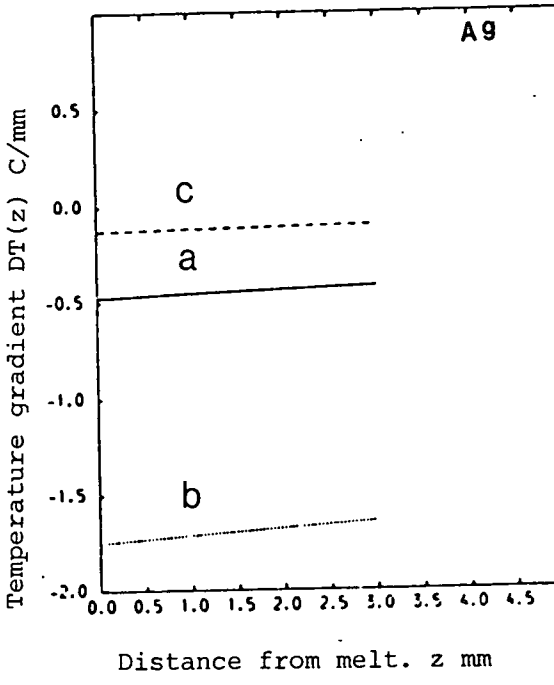

Figure 5.7 Increasing the crystal radius from .5 to 1 mm and finally to 2 mm

crystal radius a = 1mm
b = .5 mm
c = 2 mm

TABLE 5.9

Increasing neck radius

element	neck radius = .1 mm $DT_c(0)$	neck radius = .2 mm $DT_c(0)$	neck radius = .3 mm $DT_c(0)$	neck radius = .4 mm $DT_c(0)$	per cent change in $DT_c(0)$ from .4 to .1 mm
Ag	- 0.47696	- 1.56598	- 2.90850	- 4.19071	778.6
cu	- 0.58417	- 1.80609	- 3.328	- 4.79978	721.6
Ni	- 8.72141	- 10.50171	- 12.93301	- 15.62846	79.19
Si	- 15.45943	- 17.14211	- 19.38649	- 21.86757	41.45

TABLE 5.10

Increasing neck length

element	neck length = 2 mm $DT_c(0)$	neck length = 4 mm $DT_c(0)$	neck length = 6 mm $DT_c(0)$	neck length = 8 mm $DT_c(0)$	per cent change in $DT_c(0)$ from 2 to 8 mm
Ag	- 0.47696	- 0.26842	- 0.19761	- 0.16239	193.71
cu	- 0.58417	- 0.35319	- 0.27573	- 0.23786	145.59
Ni	- 8.72141	- 8.56771	- 8.54943	- 8.54698	2.04
Si	- 15.45943	- 15.38025	- 15.37576	- 15.37549	0.546

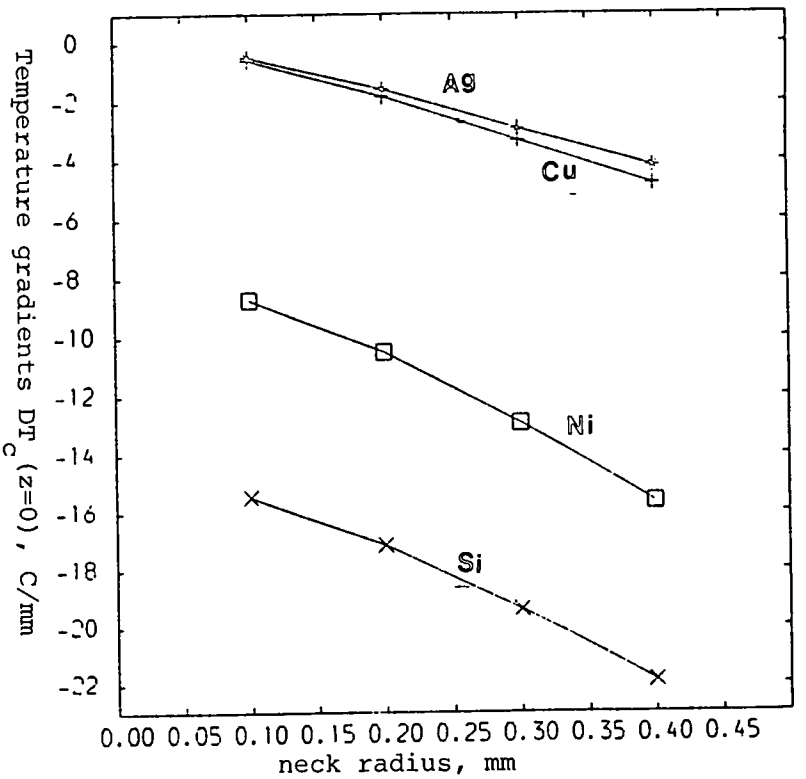

Figure 5.8 Increasing the neck radius from .1, .2, .3 and finally to .4mm for Ag, cu, Ni and Si.

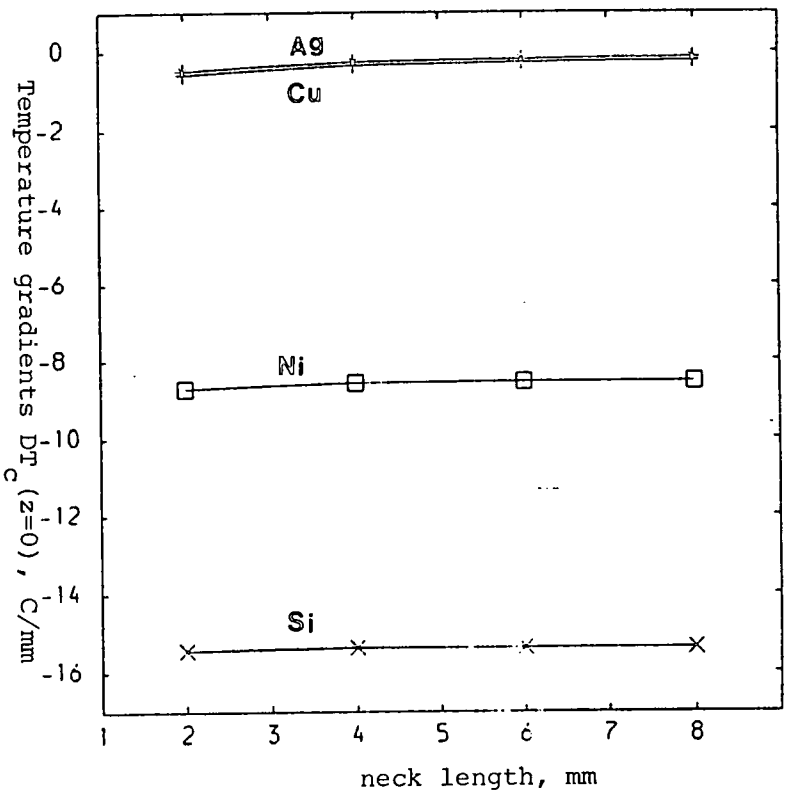

Figure 5.9 Increasing the neck length from 2, 4, 6 and finally to 8mm for Ag, cu, Ni and Si.

TABLE 5.11

Increasing crystal radius

element	crystal radius = .5 mm $DT_c(0)$	crystal radius = .75 mm $DT_c(0)$	crystal radius = 1 mm $DT_c(0)$	crystal radius = 2 mm $DT_c(0)$	per cent change in $DT_c(0)$ from .5 to 2 mm
Ag	- 1.74998	- 0.82145	- 0.47696	- 0.12749	1272.64
cu	- 2.06353	- 0.9884	- 0.58417	- 0.16313	1164.24
Ni	- 18.76881	- 12.14534	- 8.72141	- 3.50219	435.92
Si	- 30.770277	- 20.93163	- 15.45943	- 6.48199	374.70

TABLE 5.12

Increasing crystal length

element	crystal length = 3 mm $DT_c(0)$	crystal length = 6 mm $DT_c(0)$	crystal length = 9 mm $DT_c(0)$	crystal length = 12 mm $DT_c(0)$	per cent change in $DT_c(0)$ from 12 to 3 mm
Ag	- 0.47696	- 0.52433	- 0.5700	- 0.61411	28.76
cu	- 0.58417	- 0.696111	- 0.80352	- 0.90586	55.07
Ni	- 8.72141	- 15.31342	- 18.73164	- 20.23944	132.07
Si	- 15.45943	- 24.75156	- 27.88567	- 28.77459	86.13

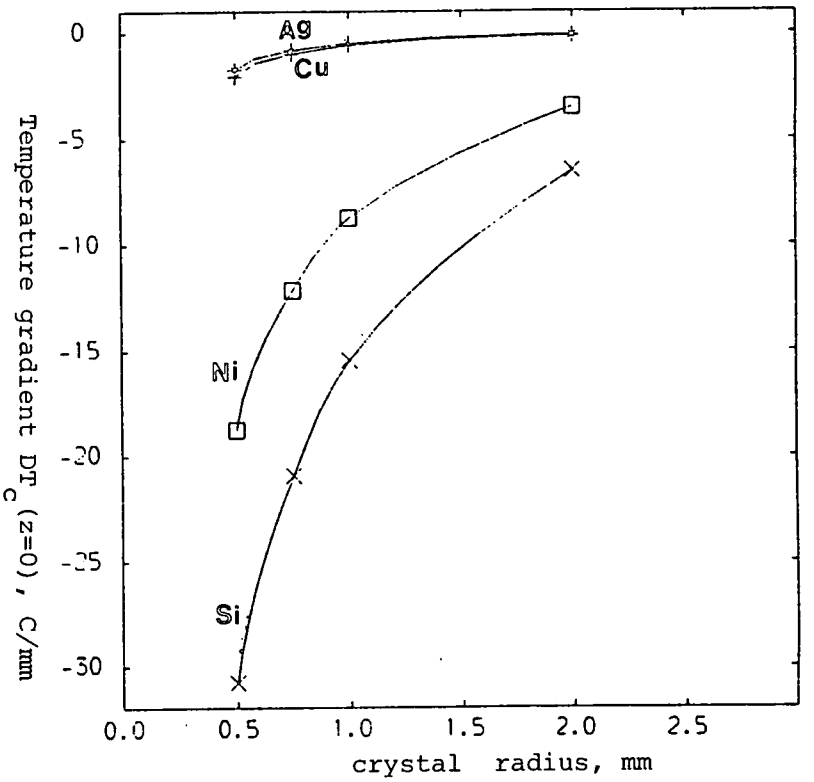

Figure 5.10 Increasing the crystal radius from 0.5, 0.75, 1 and finally to 2mm for Ag, cu, Ni and Si.

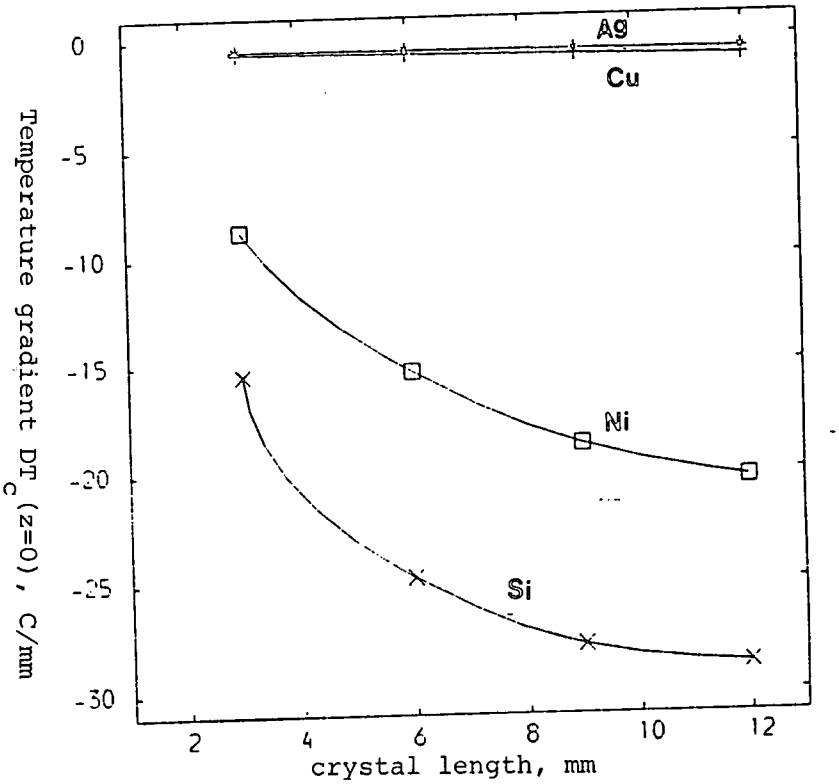

Figure 5.11 Increasing the crystal length from 3, 6, 9 to 12mm for Ag, cu, Ni and Si

TABLE 5.13

crystal radius mm	crystal length = 6 mm $DT_c(0)$	crystal length = 10 mm $DT_c(0)$
0.5	- 26.62	- 29.46
0.75	- 19.54	- 23.28
1.0	- 15.31	- 19.38
1.9	- 10.47	- 14.53
2.0	- 7.76	- 11.55

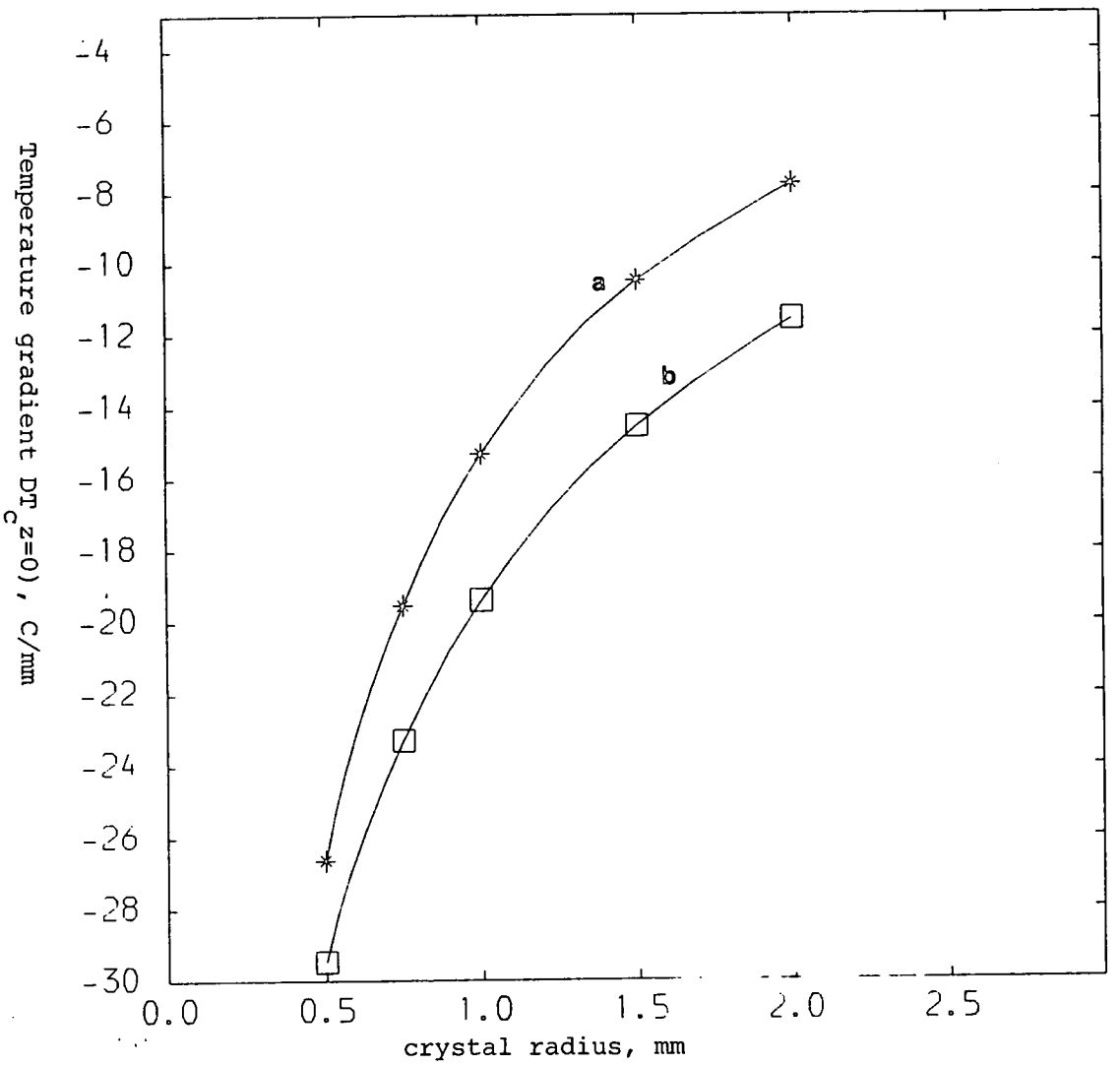

Figure 5.12 Effect of Ni crystal radius

crystal length a = 6mm
b = 10mm

CHAPTER SIX

A DESCRIPTION OF CZOCHRALSKI METHOD FOR SINGLE CRYSTAL GROWTH

6.1 Introduction

As stated in the Introduction, this method has been used widely to grow semi-conductor material such as silicon and also it has been used for growing metal single crystals.

6.2 Equipment

The equipment used for Czochralski growth of nickel is shown in Figure 6.1.

(A) A means of heating the melt:- both resistance heating and radio frequency heating are the main heating means used. The advantages of R-F heating are good visibility, which leads to good control of perfection, and the stirring action, while the advantage of resistance heating is the low initial cost due to its simplicity (Okkense, 1959).

(B) A means of containing the melt:- this requires that it should be conductive in order to couple with the radio frequency field, does not interact with the melt, and should be of high purity. The most common material used is high purity graphite. If it does interact with the melt such as Al or Ni, an alumina crucible is used, but since it does not couple with the r-f field, we use a graphite susceptor.

(C) A mechanism for holding, rotating the crystalline rod while withdrawing it from the melt; and

(D) A means of preventing the melt from reacting with the air by surrounding the growth region with inert gas

Figure 6.1a Growth region.

CHZOCRALSKI PULLING SYSTEM

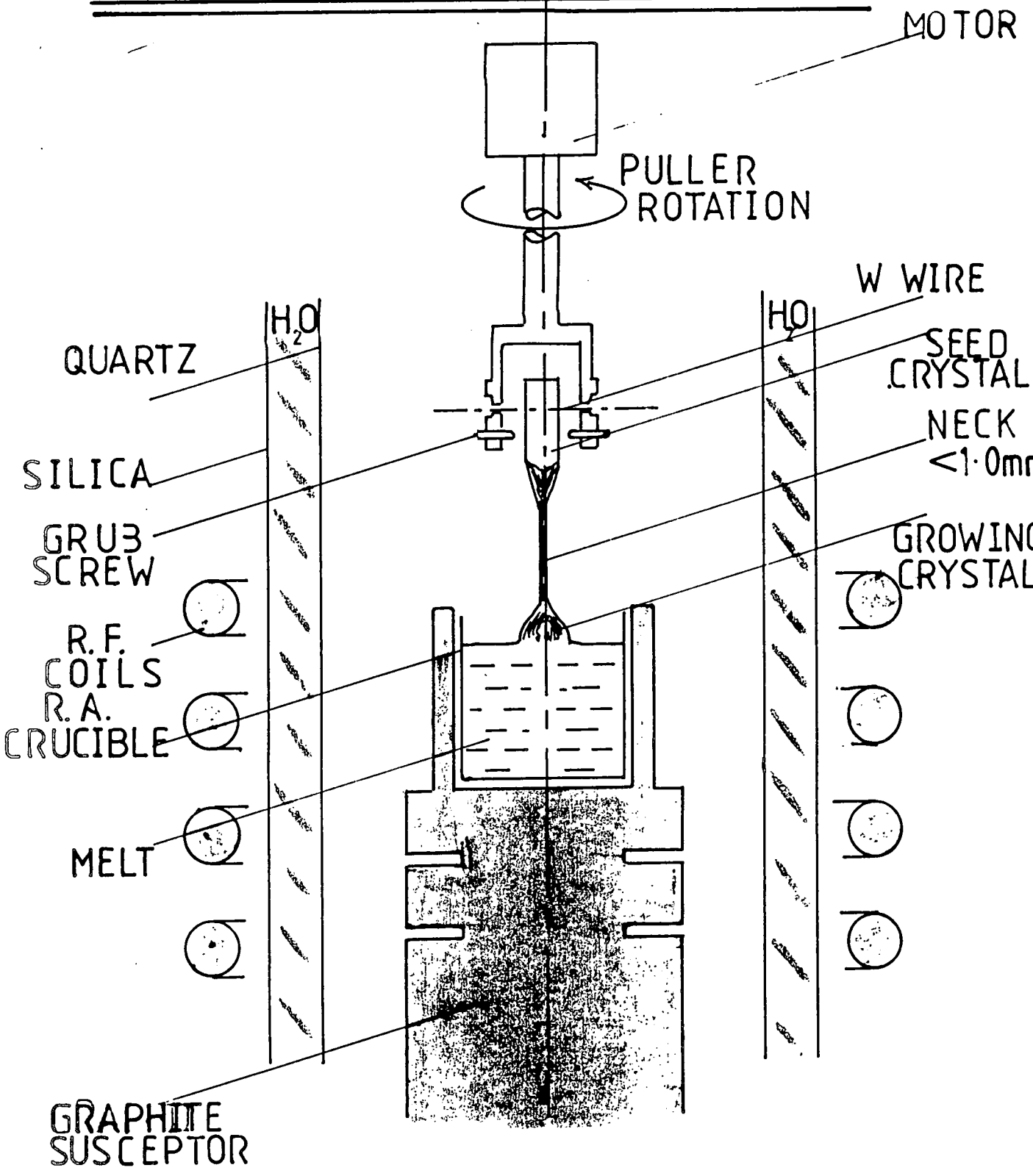

Figure 6.1b

such as Argon, which should be of high purity, or by using a vacuum. This involves two tubes and there is water running between them to prevent them from cracking during experiments.

6.3 Experimental procedure

The experimental procedure is divided into two main parts. Firstly, growing the crystal. Secondly, examining them by using X-ray topography. For the latter part a high quality single crystal should be obtained, so we use the Czochralski technique which gives a high quality single crystal. For well known reasons, the crystal should not be touched by any object during the growth process except its seed at one end and the melt surface at the other end. Also during handling (contact with other objects should be avoided) to avoid introducing any strain or damage to the crystal. The diameter of the crystal and the neck can be controlled by varying the power due to the good visibility possible in this experiment. The main disadvantage of this technique is that we have to melt our charge in a crucible which may act as a source of contamination.

The basic principle of the pulling of single crystal by the Czochralski method is as follows:-

Firstly, the system is evacuated because the presence of oxygen will lead to the formation of an oxide layer on the top of the melt.

To evacuate the system we should follow this procedure (Figure 6.2):-

1. Water is on.
2. Close A & B.
3. Check diffusion closed, butterfly closed (up) and air admit closed.

4. Open roughing valve.
5. Switch on vacuum pump then diffusion pump.
6. Switch on pirani gauge

   Wait until vacuum reaches 10^{-1} (½ hour)

   When vacuum reaches to 10^{-1} torr.

1. Close roughing valve.
2. Open diffusion valve
3. Open butterfly valve (down)
4. Switch on penning gauge scale

   Wait until vacuum reaches 10^{-1} torr.

1. Close butterfly valve (up), switch off penning.
2. Open gas cylinder.
3. Open valve A slowly

   When the system is full close A

   Close diffusion valve then open roughing valve until vacuum reaches 10^{-1}

   then re-open diffusion after you close roughing and open butterfly valve (down)

   wait until 10^{-4}

1. Close butterfly valve.
2. Open gas cylinder and valve A then valve B to regulate flow of argon.
3. Put the diffusion pump heater off and start growing.
4. After the diffusion pump heater is cooled put the vacuum pump off, close diffusion valve and open air valve.

Next comes the growing of the crystal.

The power was increased slowly to melt the polycrystalline rod which was held in the crucible. The polycrystalline rods should be of high purity and their surfaces cleaned with running water then dilute nitric acid (30% nitric

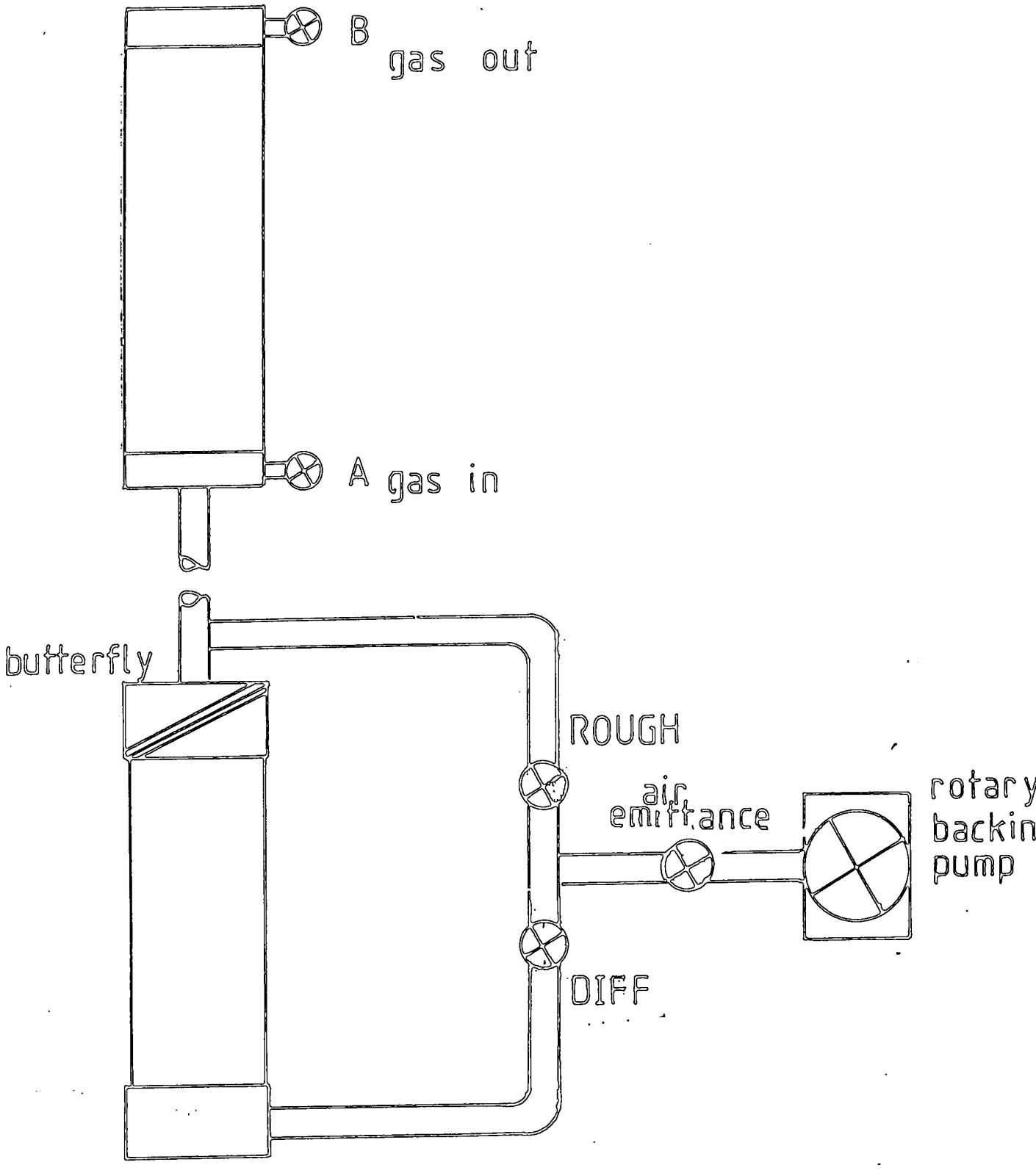

VACCUM PUMPING SYSTEM
BRIDGEMAN 365

Figure 6.2

acid + 70% water) and finally with methanol before they are used. The clean melt is an important factor in improving the quality of the crystal and any impurity present on the surface from the melt or from the tube (which should be clean before being evacuated) reduces the quality of the crystal.

When the polycrystalline rod is melted and the melt is thermally homogeneous, the single crystal or polycrystalline seed is dipped partially into the melt, sufficient time should be given to ensure complete melting of the dipped part and removal of possible contaminants which may produce dislocations (Dash, 1959).

It is then slowly withdrawn vertically with respect to the melt. High pulling speed leads to higher dislocation density while the reduction of the pulling speed will give lower dislocation density (Tanner, 1973). Kamada (1981) states that pulling with high speed changes the solid liquid interface and raises the thermal stress at the interface.

While we pull the rod we rotate it. The rotation will stir the melt and so affect both the thermal and solute distribution (Brice, 1968). Ekyo Kyroda et al. (1984) states that when the crystal rotation is reduced there will be a decrease in mocrodefect density.

The diameter of the crystal during its initial growth should be kept as small as possible. This requires that the temperature of the melt is increased slowly until a good neck is reached, following which it is extended. Producing a small neck will minimize the thermal gradient, also using an after-heater reduces the radial temperature gradient (Sworn and Brown 1972). Dash (1959) states that the neck will provide an opportunity for dislocations to grow out. Also (Buckley-

Golder and Humphreys 1979) states that the neck acts as an effective thermal resistance. Thus the heat transfer will be low as the neck is long.

After that the melt temperature is lowered to grow the crystal by decreasing the radio frequency power. The crystal should not be of a large diameter, the interface shape will be nearly flat if the crystal radius is small (Tetsuy and Nobuyki, 1969). Also for a thick crystal the heat flow increases while in the thin crystal the radiation loss is small which decreases the heat flow (van der Hart and Velhoff, 1981).

When the desired crystal length has been reached the temperature is slowly lowered to decrease the diameter gradually. This is to avoid the thermal shock which causes plastic deformation in the lower part of the crystal (Zelehner and Humber 1982).

After the crystal has become free from the melt, the temperature of the melt is lowered to room temperature. The cooling rate should be low to avoid dislocation generation by thermal stress or by vacancy condensation.

Finally the system is switched off leaving the water running to cool the system. The crystal is not moved until everything has cooled down. The crystal should be handled very carefully during its removal and cutting.

Secondly, the crystal is examined by using the Laue method to see if it is a single crystal.

Laue method as it is described by Laue atlas (1973) is used to determine the orientation and the symmetry of the crystals.

The X-ray beam is directed onto the surface of a crystal

which is fixed by soft wax on the top of the goniometer. The diffracted beams will form the diffraction pattern on the polaroid film which is placed between the source and the crystal, to show the structural properties of the crystal. If the crystal orientation is not known we will try to make the major spot to be at the centre of the next Laue pattern by tilting or rotating the sample.

CHAPTER SEVEN

RESULTS AND DISCUSSION

7.1 Copper

Single crystals of copper were grown under an argon atmosphere, Figure (7.1). Table (7.1) shows the pulling, rotation and power used. The Czochralski method was used to grow a single crystal from a polycrystalline seed and from <321> orientation. The crystal was able to be pulled directly from the graphite crucible, but copper crystals could not be grown under vacuum due to the sublimation of copper onto the walls of the silica tube. They were therefore grown under an argon atmosphere.

First of all the melting point of copper had to be found but a small neck could not be grown because of table vibrations, also the seed was not perpendicular to the melt. When the rod was rotated it made a circular motion and did not rotate at the centre of the melt. Sometimes when the power was decreased to grow a crystal, the melt was frozen and at other times the crystal was very small (Table 7.2). The rotation was stopped once, due to the dirt inside it.

Finally, single crystal <321> orientation dropped into the melt so after that a tungsten wire was used which was passed through the chuck and the rod to hold the crystal.

Single crystals were successfully grown from a polycrystalline seed and from <321> orientation. Some of these crystals were given to Dr. Sheene from Strathclyde University.

Czochralski method was used to grow dislocation free copper single crystal by Sworn and Brown (1972) under an argon atmosphere. They found that the diameter of the neck between the seed and the crystal had a great effect

on the quality of the crystal, and that the absence of an after heater will reduce the perfection of the crystal. Fehmer and Uelhoff (1972) state that they had grown single crystals of copper by this method and these crystals were free from dislocations.

7.2 Aluminium

Aluminium single crystals were grown by this method. The first one was not a single crystal, Figures (7.2, 7.3), Table (7.3). The second one by making a good neck was a single crystal, Figure (7.4), Table (7.4).

Single crystals of aluminium were grown by Howe and Elbaum, (1962) under a helium atmosphere.

7.3 Nickel

The first crystal grown was not a single crystal because the neck part was short, Figure (7.5). The Table (7.5) shows the power, pulling and rotation used.

The second crystal was a high quality single crystal having been grown by this technique from a polycrystalline seed. The neck was thinner and longer than the first one, and the cooling was decreased slowly until the melt was cooled down, Figure (7.6). This crystal was examined at Daresbury Laboratory using synchrotron radiation, and domain walls could be seen, Figure (7.7). Table (7.6) shows the power, pulling and rotation used.

The third crystal was also single. The neck was 1mm in diameter and the crystal was 7mm in length and 2.8mm in diameter. Cooling was decreased more slowly, Figure (7.8). Table (7.7) shows pulling, rotation and the power used.

The same technique was used to grow orientated nickel single crystals. At first it was found that the melt was too bright to look at directly so safety goggles were used. After that the nickel could not be melted because the graphite susceptor lost its conductivity as it had been used for a long period previously to grow copper. Also it was found that the alumina crucible which contains the Ni melt always cracked because the fit in the graphite was so tight. Another graphite susceptor with space between graphite and alumina crucible was therefore made.

The equivalent space Δr between crucible and susceptor was calculated as $\frac{\Delta r}{r} = \Delta\alpha\ T$ where $\Delta\alpha$ is the difference in thermal expansion of alumina and graphite.

α alumina (8×10^{-6}) and α graphite (3×10^{-6}), T is the melting temperature of Ni = $1453^{o}C$ and r is the outer radius of the alumina crucible = 12.2 mm.

So another graphite crucible with a space between graphite and alumina crucible of at least r = .1 mm was made, but after a second run, the alumina crucible cracked again, as alumina is porous and when the metals key into its surface, the subsequent contraction tends to fracture the alumina.

Single crystal <111> orientation was used to grow other single crystals. The reason is stated by (Zulemner, 1983). The dislocation which only moves [111] glide planes run out of the crystal, because these planes are oblique or perpendicular to the pulling direction. This single crystal seed was made with a hole in it to pass the wire through, so it holds the single crystal and minimizes the heat

transformation. This was done by a spark machine which reduced the damage.

The single crystal Figure (7.9) Table (7.8) was grown from the single crystal seed having <111> orientation. The neck was 1 mm in diameter and about 2 mm in length and the crystal was 7.5 mm in length and 1.2 mm in diameter. Table (7.9) shows the pulling, rotation and power used to grow single crystals Figure (7.10). The neck was 1 mm in diameter and about 2 mm in length and the crystal was 5.5 mm in length and 1 mm in diameter.

The same technique was used to grow this crystal which is not single. That is due to the neck having been bent during the cutting of the crystal Figure (7.11). The neck was 1 mm in diameter and about 2 mm in length and the crystal was 6 mm in length and 1.8 mm in diameter. Table (7.10) shows the pulling, rotation and power used.

Single crystal, Figure (7.12) was also grown from the single crystal seed. The neck was 1 mm in diameter and about 2 mm in length and crystal was 5 mm in length and .9 mm in diameter, the Table (7.11) shows the pulling rotation and power used.

Table (7.12) shows pulling, rotation and the power used. The neck was 4.3 mm in length varying from .84 mm to .6 mm in diameter and crystal was 5 mm in length and .8 mm in diameter. The crystal was examined at Daresbury Laboratory using Synchrotron radiation, Figure (7.13).

A further single crystal of nickel, Figure (7.14) has also been grown by this method, table (7.13) shows the pulling, rotation and power used during this growth.

This sample has been examined by synchrotron radiation in transmission, Figure (7.15a) and reflection Figure (7.15b) domain walls can be seen in Figure (7.15b).

Magnetic field was applied to see their movement, but they were immobile up to 237 x 10^{-4} Tesla.

Nickel single crystals, with low dislocation density were grown by Kuriyama et al. (1978). They have grown nickel single crystal with low dislocation density, using the same techniques. They grew single crystals 2 to 3cm in diameter by 12cm to 16cm in length with neck slightly less than 1mm in diameter. They used an acid saw to cut the crystal in slices, then they polished them on an acid polishing shell. They found that a bottleneck is essential for good crystals and <111> direction gave better quality than <110> and <100> direction. They state that by X-ray topography they were able to see the changes in the domain configuration as an external magnetic field was applied.

The crystals which were obtained at Durham University are more perfect than those obtained by Kuriyama et al. (1978). The crystals were examined intact and not in slices. Some of these crystals were sent to Strathclyde University.

7.4 Conclusion

Single crystals of aluminium, copper and nickel can be grown by Czochralski technique.

Copper single crystals can be grown directly from the graphite crucible while aluminium and nickel should be melted inside the alumina crucible to prevent interaction with the graphite crucible.

The chamber should be clean and evacuated first, the presence of oxygen will lead to the formation of an oxide layer on the top of the melt.

The neck should be present before growing the crystal and care should be taken to prevent it from bending during cutting.

The position of the crucible should be taken into account. The lower three rings of the R-F coil should surround the melt. If the crucible is high the top of the melt will solidify, if it is very low, the base of the crucible will solidify.

TABLE 7.1

Pulling (mmph)	Rotation (rph)	Volt	time h:m
2	2.8	138.9	12:20
4	2.8	137.1	12:25
4	2.8	135.2	12:30
4	2.8	168.4	12:32
4	2.8	159.4	12:40
4	2.8	150.9	12:45
Decrease the power to grow crystal			
2	2.8	126.3	13:35
2	2.8	128.0	13:35
Increase the power slowly to finish growth procedure.			

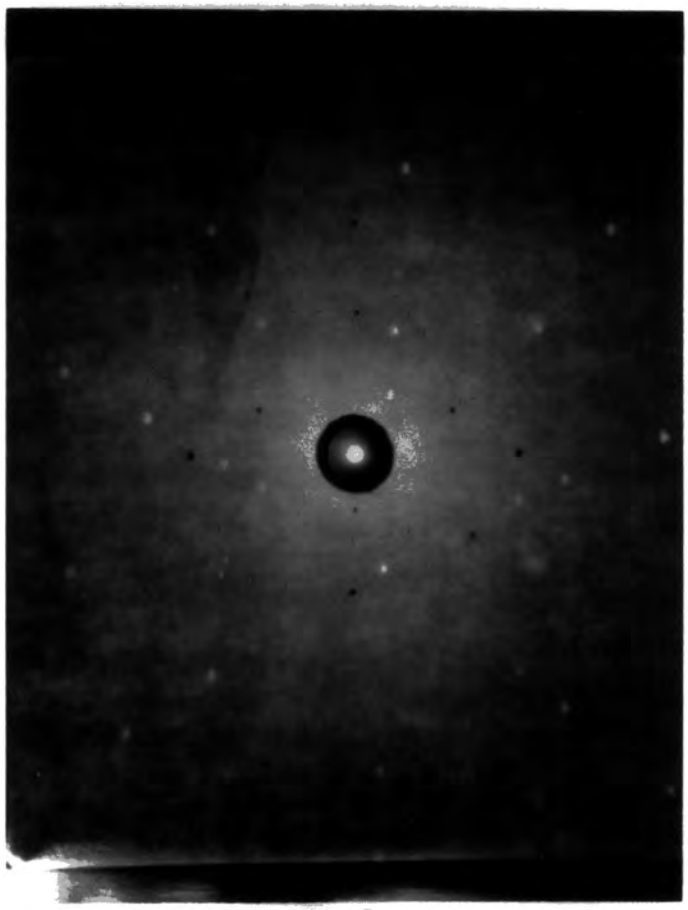

7.1

Figure 7.1 Laue pattern of a <111> Cu single crystal. It has single spots, 3 fold symmetry through the axis.

TABLE 7.2

Pulling (mmph)	Rotation (rpm)	volt	time h:m
2	2.8	135.2	14:15
Decrease the power to grow crystal			
2	2.8	124.5	14:35
2	2.8	124.1	14:50
Crystal with small diameter			
2	2.8	131.6	15:55
Decrease the power to grow crystal			
2	2.8	121.8	15:05
The melt is frozen			
2	2.8	131.6	15:35
Decrease the power to grow crystal			
2	2.8	123.2	15:40
Crystal with large diameter			

TABLE 7.3

Pulling (mmph)	volt	time h:m
2	118.2	13:50
Decrease the power to grow crystal		
2	105.6	14:15
2	105.9	14:38
Increase the power slowly to finish growth procedure		

TABLE 7.4

Pulling (mmph)	volt	time h:m
2	117.9	10:30
2	118.2	11:00
2	118.5	12:12
Decrease the power to grow crystal		
2	105.6	12:31
2	105.9	12:45
Increase the power slowly to finish growth procedure		

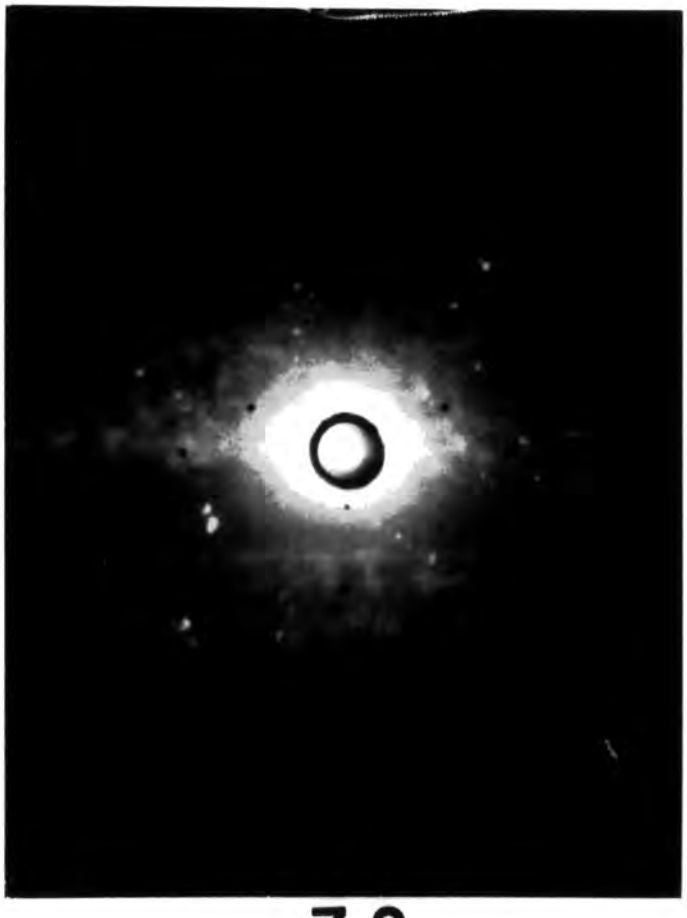

7.2

Figure 7.2 First specimen. It is not single as the spots are double.

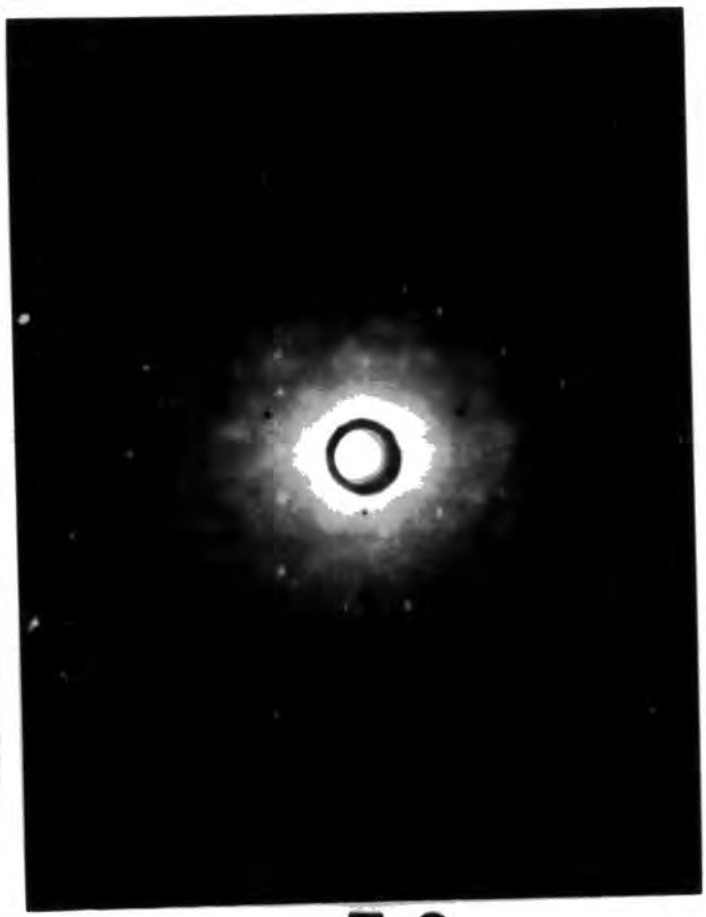

7.3

Figure 7.3 In the same specimen you can see a double spot.

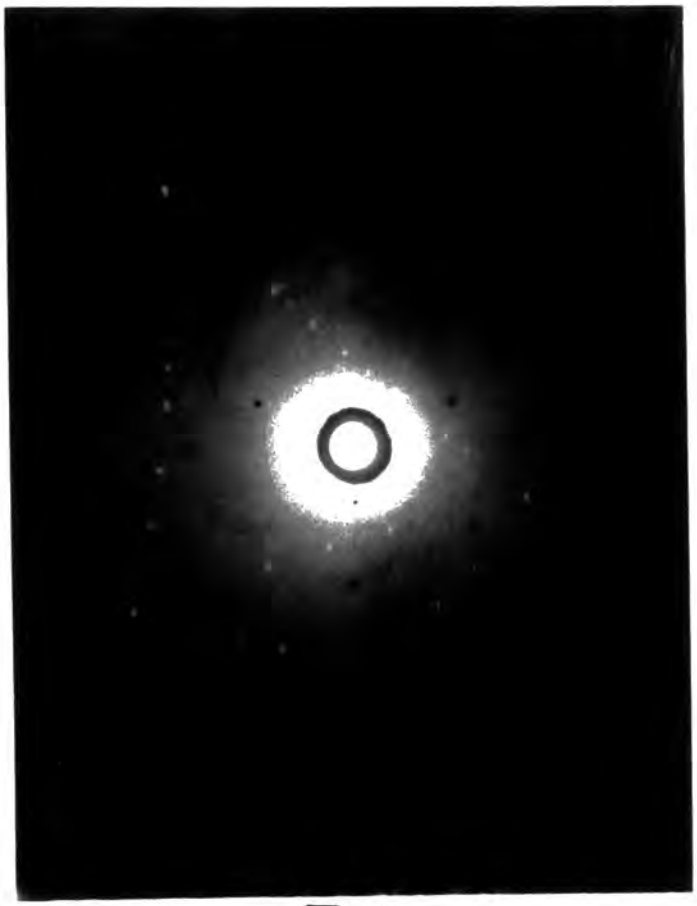

7.4

Figure 7.4 Laue pattern for single crystal aluminium of unknown orientation.
The spots are sharp and single.

TABLE 7.5

Pulling (mmph)	Rotation rph	volt	time h:m
8	1.4	227.8	10:15
8	1.4	228.4	10:28
8	1.4	229.1	10:30
8	1.4	229.6	10:35
8	1.4	230.3	10:40
8	1.4	231.	10:50
Decrease the power to grow crystal			
2	1.4	218.6	11:25
2	1.4	219.2	11:40
Increase the power slowly to finish growth procedure			

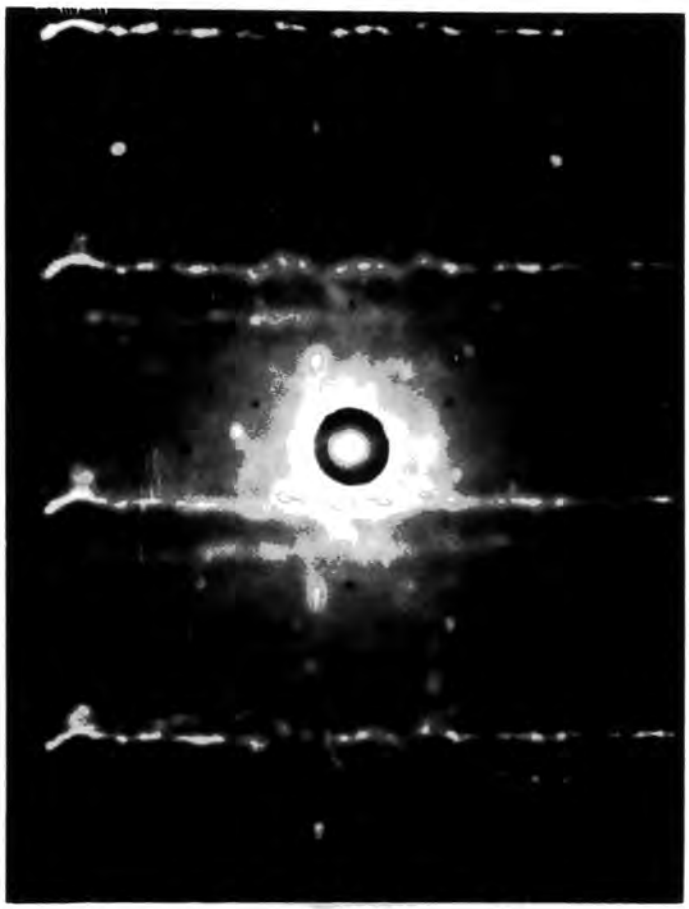

7.5

Figure 7.5 Laue pattern for the first specimen. The double spots indicate that the crystal is not single.

TABLE 7.6

Pulling (mmph)	Rotation rpm	volt	Time h:m
4	1.4	227.8	12:20
6	1.4	227.8	12:30
6	1.4	228.4	12:33
8	1.4	239.1	12:40
8	1.4	229.6	12:46
8	1.4	230.3	12:56
8	1.4	231.	13:02
Decrease the power to grow crystal			
2	1.4	218.6	13:10
2	1.4	219.2	13:29
Increase the power slowly to finish growth procedure			

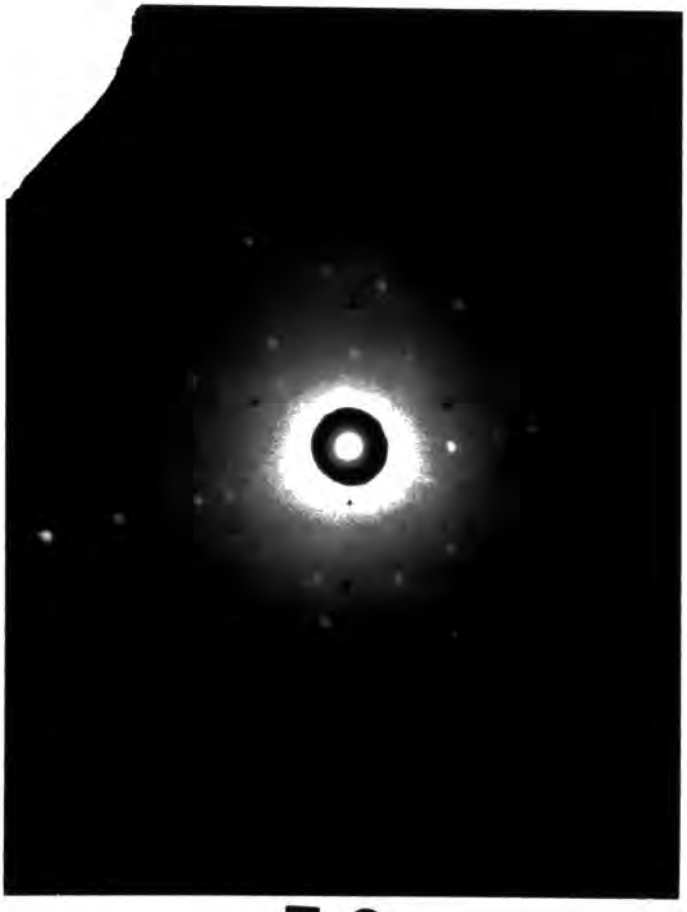

7.6

Figure 7.6 Laue pattern for the second specimen, we can that it is a <100> single crystal, the spots are sharp and single.

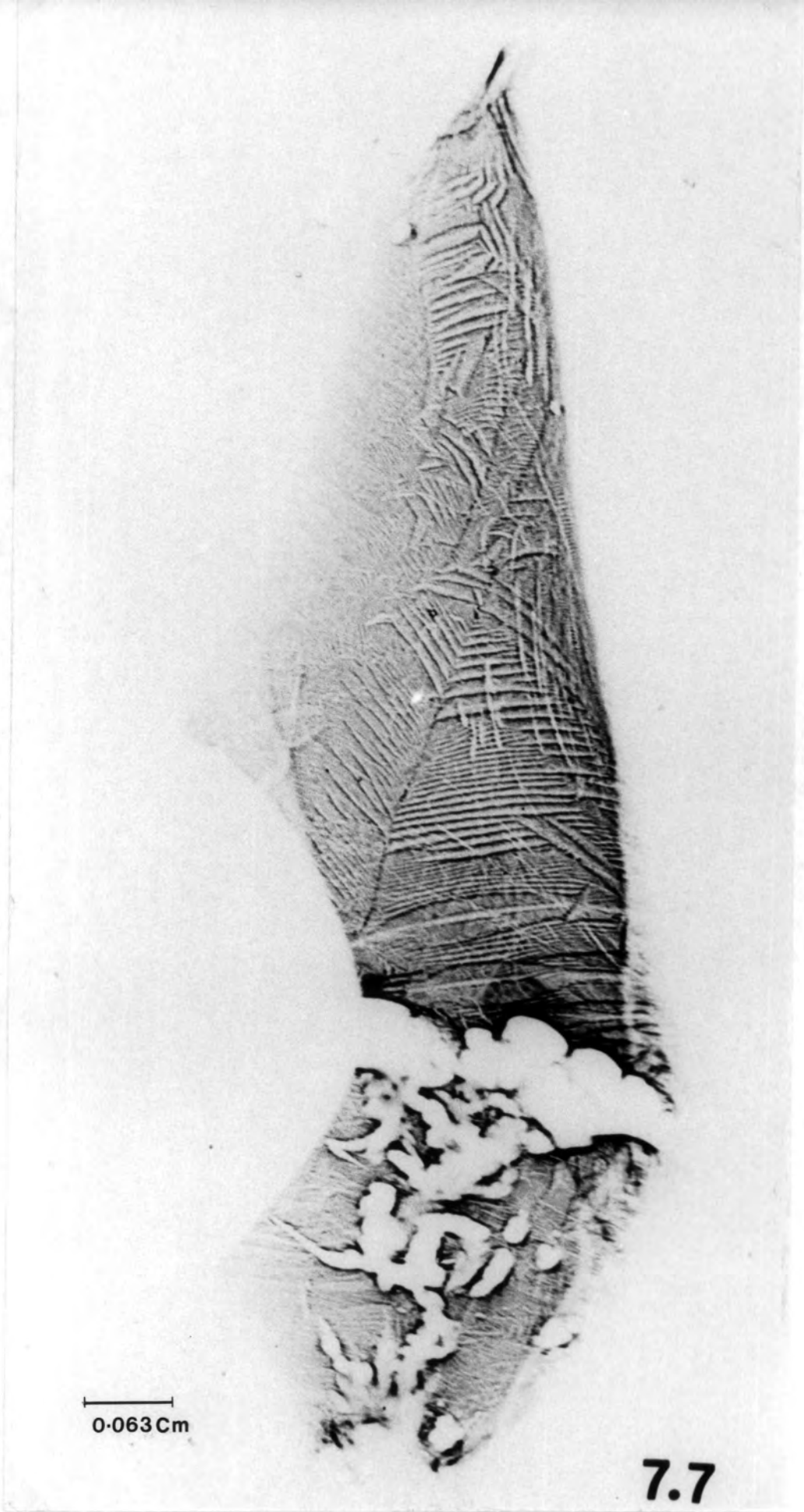

Figure 7.7 Synchrotron topographs of Ni crystal taken with the white beam radiation at Daresbury. We can see the domain walls which are close together, the light area is a large mis-orientation probably due to the impurity which occurs during the growth.

TABLE 7.7

Pulling (mmph	Rotation (rpm)	volt	Time h:m
6	1.4	221.6	11:38
6	1.4	222.3	11:50
6	1.4	222.9	11:57
6	1.4	223.5	12:06
4	1.4	224.1	12:13
4	1.4	224.7	12:21
2	1.4	225.3	12:26
2	1.4	225.9	12:28
To grow the crystal			
2	1.4	213.9	12:30
2	1.4	214.5	12:45
Increase the power slowly to finish the growth process.			

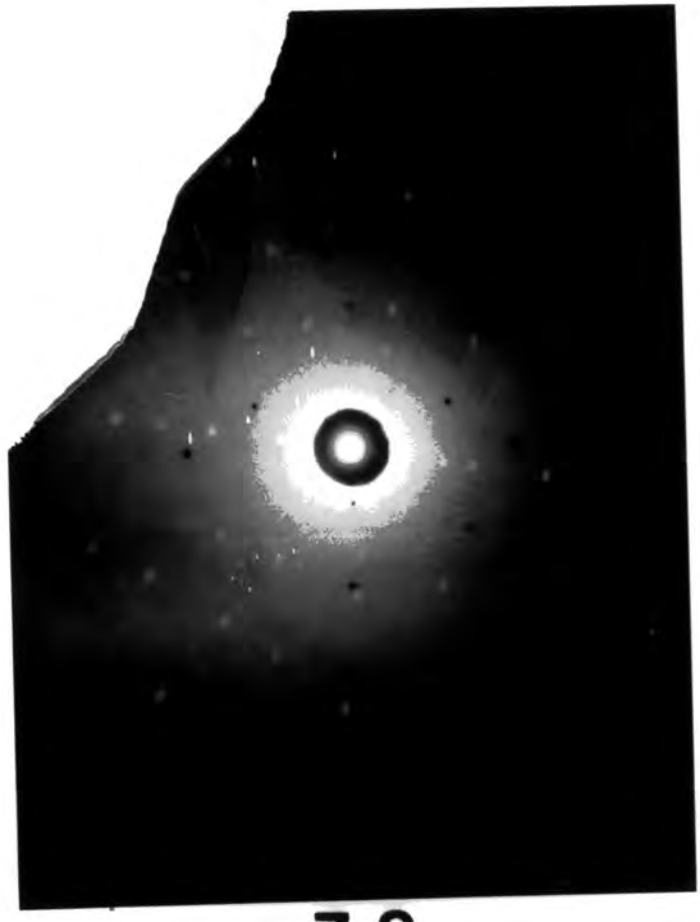

7.8

Figure 7.8 Laue pattern for the third specimen, we can see that it is a <100> single crystal.

TABLE 7.8

Pulling (mmph)	Rotation (rpm)	volt	Time h:m
6	1.4	221.0	11:05
6	1.4	221.6	11:10
6	1.4	222.3	11:15
6	1.4	222.9	11:19
6	1.4	223.5	11:24
6	1.4	224.1	11:29
2	1.4	224.7	11:33
2	1.4	225.3	11:37
2	1.4	225.9	11:41
2	1.4	226.6	11:43
2	1.4	227.2	11:45
To grow the crystal			
2	1.4	215.1	11:47
2	1.4	215.6	12:02
Increases the power slowly to finish the growth process			

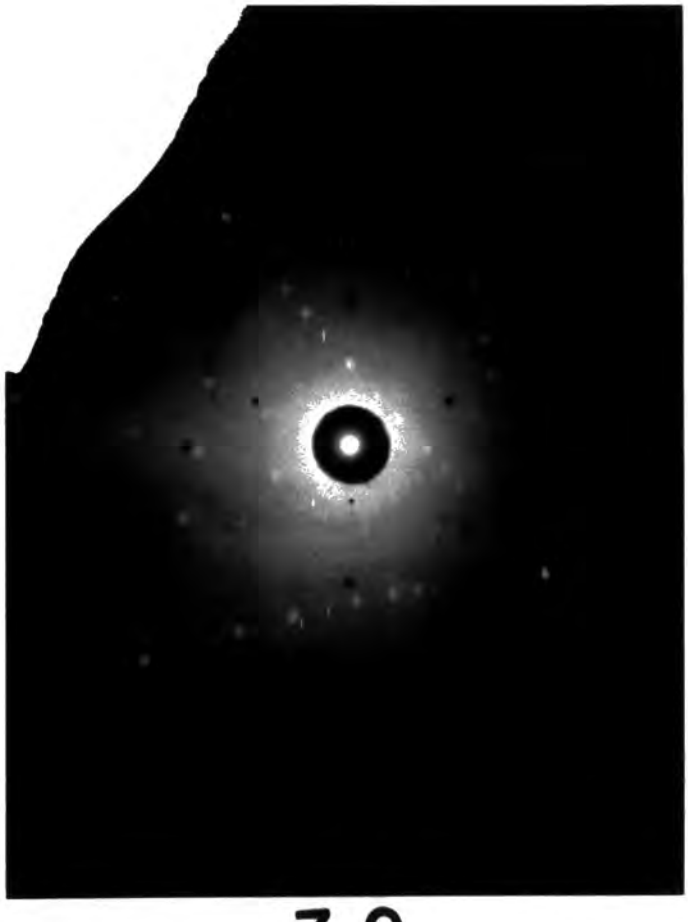

7.9

Figure 7.9 Laue pattern for <111> nickel single crystal.

TABLE 7.9

Pulling (mmph)	Rotation (rpm)	Volt	time h:m
4	1.4	221.6	14:01
4	1.4	222.3	14:05
4	1.4	222.9	14:08
2	1.4	223.5	14:12
2	1.4	224.1	14:15
2	1.4	224.7	14.18
To grow the crystal, decrease the power			
2	1.4	215.1	14:20
2	1.4	215.6	14:35
Increase the power slowly to finish the growth process			

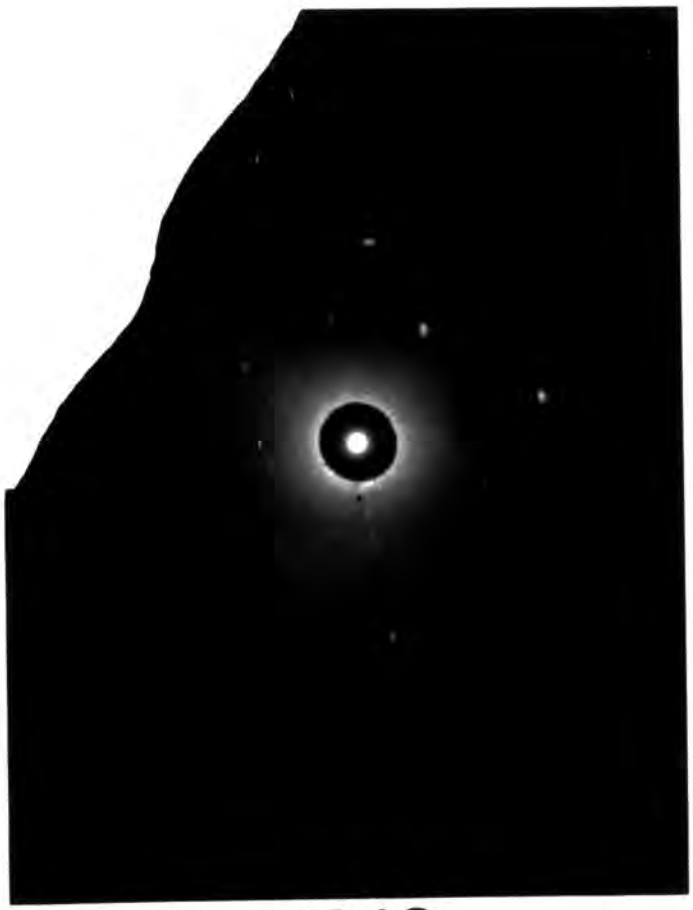

7.10

Figure 7.10 Laue pattern for nickel single crystal.

TABLE 7.10

Pulling (mmph)	Rotation (rph)	Volt	Time h:m
4	1.4	222.3	11:50
2	1.4	222.9	11:57
2	1.4	223.5	12:02
2	1.4	224.1	12:04
2	1.4	224.7	12:06
To grow the crystal, decrease the power			
2	1.4	215.1	12:08
2	1.4	215.6	13:23
Increase the power to finish the growth process			

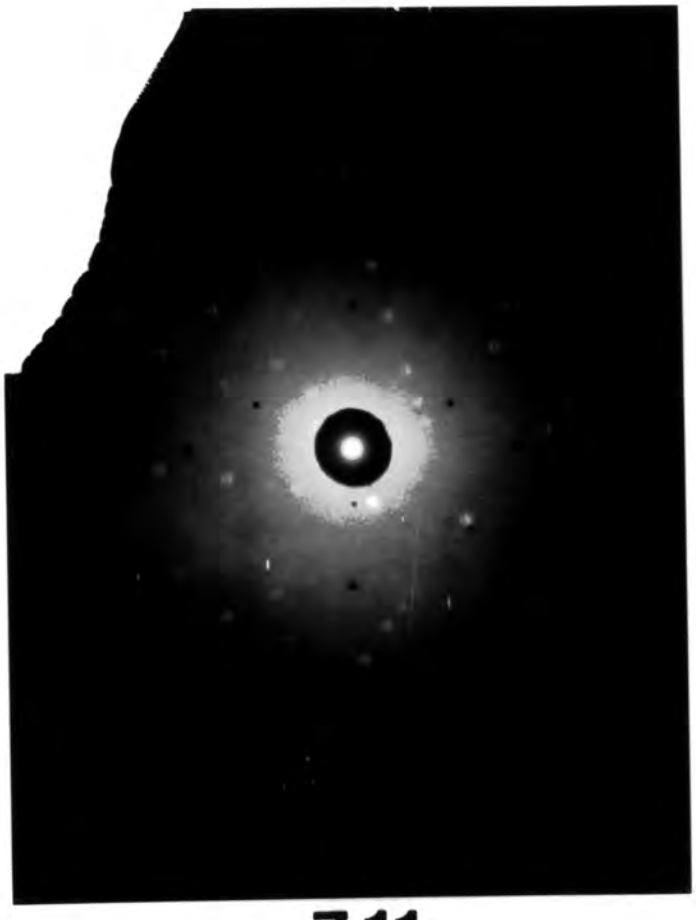

7.11

Figure 7.11 It is not single as the spots are double.

TABLE 7.11

Pulling (mmph)	Rotation (rpm)	Volt	Time h:m
4	1.4	221.6	13:17
4	1.4	222.3	13:23
2	1.4	222.9	13:28
2	1.4	223.5	13:32
2	1.4	224.1	13:34
Decrease the power to grow the crystal			
2	1.4	215.1	13:36
Increase the power slowly to finish growth process			

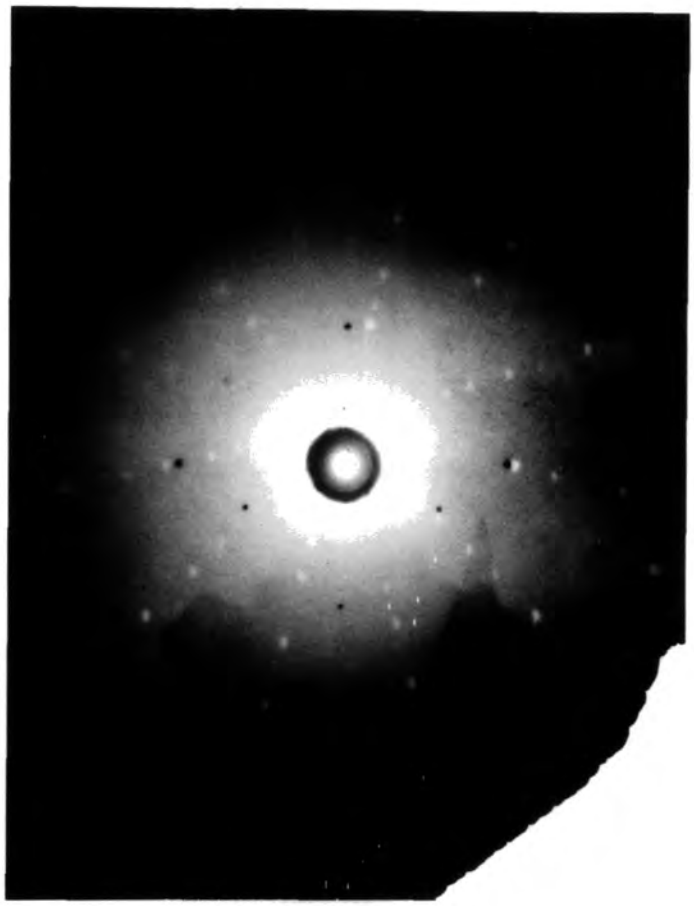

7.12

Figure 7.12 Laue pattern for <111> nickel single crystal.

TABLE 7.12

Pulling (mmph)	Rotation (rpm)	Volt	Time h:m
2	1.4	219.8	13:15
2	1.4	220.4	13:18
2	1.4	221.0	13.21
2	1.4	221.6	13:24
2	1.4	222.3	13:28
2	1.4	222.9	13:31
Decrease the power to grow the crystal			
2	1.4	215.1	13:32
2	1.4	215.6	13:47
Increase to finish the crystal growth			

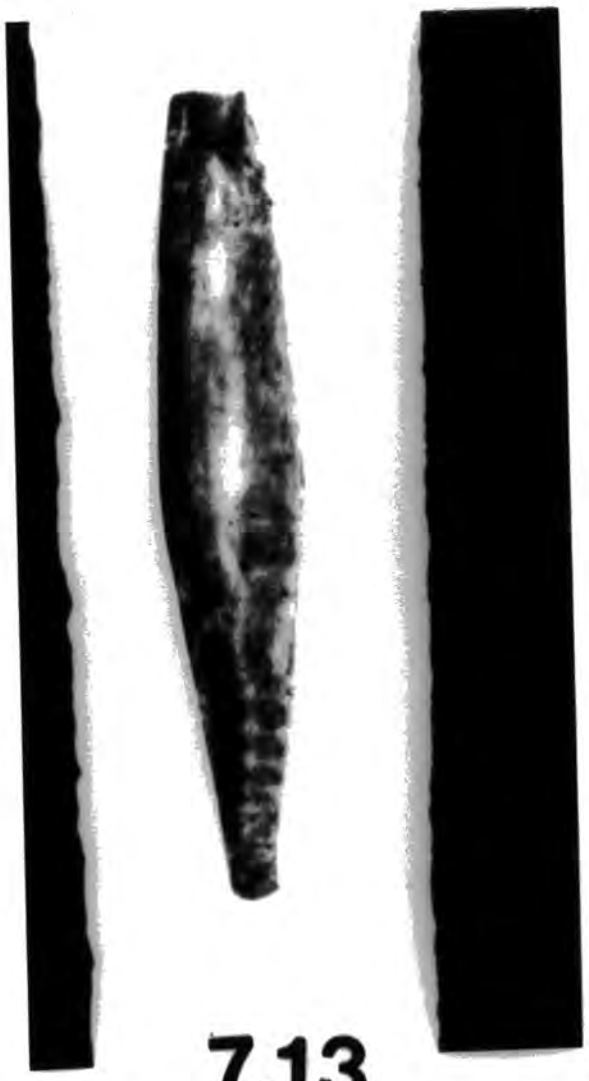

7.13

Figure 7.13 Transmission topographs of nickel crystal taken with the white beam radiation at Daresbury. Dislocation bands can be seen at the bottom.

TABLE 7.13

Pulling (mmph)	Rotation rpm	volt	time h:m
4	1.4	223.5	12:51
2	1.4	224.1	12:59
2	1.4	224.7	13:05
2	1.4	223.5	13:08
2	1.4	222.3	13:14
2	1.4	222.9	13:19
Decrease to grow the crystal			
2	1.4	213.9	13:22
2	1.4	214.5	13:37
Increase the power slowly to finish the growth process			

Figure 7.14 Laue pattern for <111> nickel single crystal.

Figure 7.15 White synchrotron X-ray radiation topographs of nickel single crystal. Domain structure can be seen and the deformed region caused by cutting can be picked out.

Figure 7.15a Transmission topograph.

Figure 7.15b Surface reflection topograph.

APPENDIX A

```
  10 MODE 0
  20 *DRIVE 0
  30   DIM E1$(10),E2$(10),C$(3),TM(10),TA(10),E(10),K(10)
  40   DIM A(3),L(3),R(3),HR(2),BIOT(2,3)
  50   DIM C(2,6),Z(200),TZ(2,200),DTZ(2,200)
  60 C$(1)="Crystal":C$(2)="neck":C$(3)="seed"
  70  RESTORE 1430
  80 READ ELEMENT
  90    FOR I=1 TO ELEMENT: READ E1$(I),E2$(I),TM(I),TA(I),E(I),K(I):NEXT I
 100    FOR J=1 TO 3:READ R(J),L(J):A(J)=PI*R(J)^2:NEXT J
 110    L(2)=L(1)+L(2)
 120    L(3)=L(2)+L(3)
 130 CLS:@%=0:PRINT
 140 PRINT TAB(15);"A theoretical study of tepmerature distributions"
 150 PRINT TAB(15);"      during Czochralski crystal growth"
 160 FOR I=1 TO 3:PRINT:NEXT I
 170 PRINT TAB(10);"Calculations can be made for one of the following elements
"
 180 PRINT
 190      FOR I=1 TO ELEMENT
 200           PRINT TAB(27);I;" ..... ";TAB(37);E1$(I);TAB(52);E2$(I)
 210      NEXT I
 220 PRINT:PRINT:INPUT "                                    Your Option Please : ";N
 230 E1$=E1$(N):E2$=E2$(N):TM=TM(N):TA=TA(N):E=E(N):K=K(N)
 240  T1=TM+273.150:T2=TA+273.150:RHU=5.66956E-14:REM (W/mm^2/deg^4)
 250  HR(1)=RHU*E*(T1^3+T1^2*T2+T1*T2^2+T2^3):REM (W/mm^2/C)
 260 PROCtable1
 270 PRINT
 280 INPUT "                    Factor for high radiation  ";FAC
 290 HR(2)=HR(1)*FAC
 300 PROCtable2
 310  PRINT:PRINT:PRINT "                                SPACE PAR TO CONTINUE   ";
A=GET
 320 CLS:PROCtable3
 330 PRINT:PRINT:INPUT"              Do you want to change any of these valu
s  (Y/N) ";ANS$
 340IF ANS$="N" OR ANS$="n" THEN 500
 350 IF ANS$="Y" OR ANS$="y" THEN 370
 360 GOTO 330
 370PRINT:PRINT
 380INPUT"   Index No. to be changed ";NI
 390 PRINT
 400 IF NI=1 THEN INPUT"   Radius of crystal = ";R(1):A(1)=PI*R(1)^2:GOTO 320
 410 IF NI=2 THEN INPUT"   Radius of neck    = ";R(2):A(2)=PI*R(2)^2:GOTO 320
 420 IF NI=3 THEN INPUT"   Radius of seed    = ";R(3):A(3)=PI*R(3)^2:GOTO 320
 430 IF NI=4 THEN INPUT"   Length of crystal = ";L(1):GOTO 320
 440 IF NI=5 THEN INPUT"   Length of neck    = ";L(2):L(2)=L(2)+L(1):GOTO 320
 450 IF NI=6 THEN INPUT"   Length of seed    = ";L(3):L(3)=L(2)+L(3):GOTO 320
 460 GOTO 380
 470 :
 480 :
 490  REM @ @ @ @ @ @ @ @ @ @ @ @ @ @ @ @ @ @ @ @ @ @ @ @ @ @ @ @ @ @ @ @ @ @ @
 500 REM
 510  REM  Calculate the BIOT NUMBERS for lwo and high radiations
 520 REM
 530 FOR I=1 TO 2
 540 FOR J=1 TO 3:BIOT(I,J)=HR(I)*R(J)/K:NEXT J
 550 NEXT I
 560 PROCtable4
```

```
570 REM
580 REM @ @ @ @ @ @ @ @ @ @ @ @ @ @ @ @ @ @ @ @ @ @ @ @ @ @ @ @ @ @ @ @ @ @ @ @ @
590REM
600  REM  Solve for the constants  C1,C2,C3,C4,C5, and C6 (both low and high)
610REM
620 FOR I=1 TO 2
630 XC=SQR(2*BIOT(I,1))/R(1):XN=SQR(2*BIOT(I,2))/R(2):XS=SQR(2*BIOT(I,3))/R(3)
640 C(I,1)=TM-TA
650 X=XC*L(1):GOSUB 710:SCC=X1:CCC=X2
660 X=XN*L(2):GOSUB 710:SNN=X1:CNN=X2
670 X=XS*L(3):GOSUB 710:SSS=X1:CSS=X2
680 X=XN*L(1):GOSUB 710:SNC=X1:CNC=X2
690 X=XS*L(2):GOSUB 710:SSN=X1:CSN=X2
700  GOTO 740
710 X1=0.5*(EXP(X)-EXP(-X))
720 X2=0.5*(EXP(X)+EXP(-X))
730 RETURN
740 ALP1=(K*A(1)*XC*CCC/SCC)-(HR(I)*(A(1)-A(2)))
750 ALP2=K*A(2)*XN*SNC
760 ALP3=K*A(2)*XN*CNC
770  ALP4=HR(I)*(A(1)-A(2))*CCC*C(I,1)-K*A(1)*XC*SCC*C(I,1)
780 BETA1=K*A(2)*XN*SNN-HR(I)*(A(3)-A(2))*CNN
790 BETA2=K*A(2)*XN*CNN-HR(I)*(A(3)-A(2))*SNN
800 EPSI=-(CSS/SSS)
810 BETA3=K*A(3)*XS*(SSN+EPSI*CSN)/(CSN+EPSI*SSN)
820 GAMA=-(BETA2-BETA3*SNN)/(BETA1-BETA3*CNN)
830 :
840 C(I,4)=(ALP4+ALP1*CCC*C(I,1))/(ALP1*CNC*GAMA-ALP2*GAMA+ALP1*SNC-ALP3)
850 C(I,3)=C(I,4)*GAMA
860 C(I,5)=(CNN*C(I,3)+SNN*C(I,4))/(CSN+EPSI*SSN)
870 C(I,2)=(CNC*C(I,3)+SNC*C(I,4)-CCC*C(I,1))/SCC
880 C(I,6)=EPSI*C(I,5)
890 NEXT I
900 PROCtable5
910 REM
920 REM @ @ @ @ @ @ @ @ @ @ @ @ @ @ @ @ @ @ @ @ @ @ @ @ @ @ @ @ @ @ @ @ @ @ @ @ @
930 REM
940FOR I=1 TO 2
950 XC=SQR(2*BIOT(I,1))/R(1):XN=SQR(2*BIOT(I,2))/R(2):XS=SQR(2*BIOT(I,3))/R(3)
960 Z%=0
970FOR J=0 TO L(1) STEP 2
980 Z%=Z%+1
990 Z(Z%)=J
1000 X=XC*J:GOSUB 710:S=X1:C=X2:TZ(I,Z%)=TA+C(I,1)*C+C(I,2)*S:DTZ(I,Z%)=XC*S*C(
I,1)+XC*C*C(I,2)
1010 NEXT J
1020 FOR J=L(1) TO L(2)
1030 Z%=Z%+1
1040 Z(Z%)=J
1050 X=XN*J:GOSUB 710:S=X1:C=X2:TZ(I,Z%)=TA+C(I,3)*C+C(I,4)*S:DTZ(I,Z%)=XN*S*C(
I,3)+XN*C*C(I,4)
1060 NEXT J
1070 FOR J=L(2) TO L(3) STEP 10
1080 Z%=Z%+1
1090Z(Z%)=J
1100 X=XS*J:GOSUB 710:S=X1:C=X2:TZ(I,Z%)=TA+C(I,5)*C+C(I,6)*S:DTZ(I,Z%)=XS*S*C(
I,5)+XS*C*C(I,6)
1110 NEXT J
1120 NEXT I
1130:
```

```
1140 PRINT:PRINT:PRINT"                                    SPACE PAR TO CONTINUE "
1150 AA=GET
1160 PROCtable6
1170 PRINT TAB(30);"SPACE PAR TO CONTINUE "
1180 AA=GET
1190CLS:PRINT:PRINT
1200PRINT TAB(10);"L  .....    Display Results  "
1210PRINT
1220PRINT TAB(10);"S  .....    Store Data in a Disk File "
1230PRINT
1240PRINT TAB(10);"N  .....    Next Element "
1250PRINT
1260PRINT TAB(10);"Q  .....    Quite "
1270PRINT:PRINT:PRINT
1280INPUT "          OPTION   ";ANS$
1290IF ANS$="Q" OR ANS$="q" THEN END
1300 IF ANS$="L" OR ANS$="l" THEN PROClist:GOTO 1190
1310 IF ANS$="S" OR ANS$="s" THEN PROCstore:GOTO 1190
1320 IF ANS$="N" OR ANS$="n" THEN GOTO 130
1330 GOTO 1140
1340 END
1350    REM  ********************************************************
1360    REM   The following internal data have been taken from
1370    REM   Physics and Chemistry Handbook, 55th edition (1977):
1380    REM        (1) Element
1390    REM        (2) Melting temperature   TM  (C)
1400    REM        (3) Ambient temperature   TA  (C)
1410    REM        (4) Emissivity             E  (at 0.65 micron)
1420    REM        (5) Thermal conductivity   K  (W/mm/C)
1430    DATA 4
1440    DATA "Copper   ","Cu",1083,983,0.1,0.342
1450    DATA "Silicon  ","Si",1410,1279,0.46,2.51E-2
1460    DATA "Nickel   ","Ni",1453,1318,0.5041,0.059
1461    DATA "Silver   ","Ag",961.9,872,0.07,0.363
1470    REM  ********************************************************
1480    REM   The adopted geometric of the MODEL :
1490    REM   -1-  Radius (mm), and Length (mm)   of CRYSTAL
1500    REM   -2-  Radius (mm)  and Length (mm)   of NECK
1510    REM   -3-  Radius (mm)  and Length (mm)   of SEED
1520    DATA 1.0,20
1530    DATA 0.15,3
1540    DATA 3,60
1550    REM  ********************************************************
1560DEF PROCtable1
1570 @%=0
1580PRINT:PRINT
1590PRINT TAB(2);"Element";TAB(20);"TM";TAB(30);"TA";TAB(40);"Emissivity";TAB(5
5);"Thermal Conductivity"
1600PRINT TAB(20);"(C)";TAB(30);"(C)";TAB(60);"(W/mm/C)"
1610PRINT
1620PRINT TAB(2);E1$;E2$;TAB(20);TM;TAB(30);TA;TAB(43);E;TAB(60);K
1630PRINT:@%=&10509
1640PRINT TAB(2);"Heat-Radiation Coefficient   HR (low radiation)  = ";HR(1);"
(W/mm^2/C)"
1650 ENDPROC
1660 DEF PROCtable2
1670PRINT:@%=20209
1680PRINT TAB(20);"Factor for high radiation = ";FAC
1690PRINT:@%=&10509
1700PRINT TAB(2);"Heat-Radiation Coefficient   HR (high radiation) = ";HR(2);"
```

```
(W/mm^2/C)"
 1710ENDPROC
 1720DEF PROCtable3
 1730@%=0
 1740FOR I=16 TO 70:PRINT TAB(I);"*";:NEXT I
 1750PRINT TAB(18);"Area (mm^2)";TAB(38);"Radius (mm)";TAB(58);"Length (mm)"
 1760FOR I=16 TO 70:PRINT TAB(I);"*";:NEXT I
 1770FOR J=1 TO 3
 1780PRINT TAB(5);C$(J);TAB(18);A(J);TAB(38);"(";J;")  ";R(J);TAB(58);"(";J+3;")
  ";L(J)-L(J-1)
 1790NEXT J
 1800FOR I=16 TO 70:PRINT TAB(I);"*";:NEXT I
 1810ENDPROC
 1820DEF PROCtable4
 1830@%=&10509
 1840PRINT:FOR J=20 TO 65:PRINT TAB(J);"-";:NEXT J
 1850PRINT TAB(20);"B(crystal)";TAB(40);"B(neck)";TAB(55);"B(seed)"
 1860FOR J=20 TO 65:PRINT TAB(J);"-";:NEXT J
 1870PRINT TAB(1);"Low radiation";TAB(20);BIOT(1,1);TAB(40);BIOT(1,2);TAB(55);BI
OT(1,3)
 1880PRINT TAB(1);"High radiation";TAB(20);BIOT(2,1);TAB(40);BIOT(2,2);TAB(55);B
IOT(2,3)
 1890FOR J=20 TO 65:PRINT TAB(J);"-";:NEXT J
 1900ENDPROC
 1910DEF PROCtable5
 1920@%=&20509
 1930PRINT:PRINT
 1940FOR I=25 TO 60:PRINT TAB(I);".";:NEXT I
 1950PRINT TAB(25);"Low Radiation";TAB(45);"High Radiation"
 1960 FOR I=25 TO 60:PRINT TAB(I);".";:NEXT I
 1970 PRINT
 1980PRINT TAB(20);"C1 ";TAB(27);C(1,1);TAB(47);C(2,1)
 1990PRINT TAB(20);"C2 ";TAB(27);C(1,2);TAB(47);C(2,2)
 2000PRINT TAB(20);"C3 ";TAB(27);C(1,3);TAB(47);C(2,3)
 2010PRINT TAB(20);"C4 ";TAB(27);C(1,4);TAB(47);C(2,4)
 2020PRINT TAB(20);"C5 ";TAB(27);C(1,5);TAB(47);C(2,5)
 2030PRINT TAB(20);"C6 ";TAB(27);C(1,6);TAB(47);C(2,6)
 2040FOR I=25 TO 60:PRINT TAB(I);".";:NEXT
 2050ENDPROC
 2060DEF PROCtable6
 2070CLS
 2080 FOR I=1 TO 10:PRINT TAB(I);"*";:NEXT
 2090 FOR I=20 TO 37:PRINT TAB(I);"*";:NEXT
 2100 FOR I=50 TO 67:PRINT TAB(I);"*";:NEXT
 2110 PRINT TAB(2);"z (mm)";TAB(25);"Tz (C)";TAB(55);"DTz (C/mm)"
 2120 PRINT TAB(22);"Low";TAB(32);"High";TAB(52);"Low";TAB(62);"High"
 2130 FOR I=1 TO 10:PRINT TAB(I);"*";:NEXT
 2140 FOR I=20 TO 37:PRINT TAB(I);"*";:NEXT
 2150 FOR I=50 TO 67:PRINT TAB(I);"*";:NEXT
 2160FOR I=1 TO Z%
 2170@%=&20109
 2180 IF Z(I)=Z(I-1) THEN PRINT:PRINT
 2190PRINT TAB(3);Z(I);TAB(20);TZ(1,I);TAB(30);TZ(2,I);
 2200@%=&20509
 2210PRINT TAB(50);DTZ(1,I);TAB(60);DTZ(2,I);
 2220NEXT I
 2230 FOR I=1 TO 67:PRINT TAB(I);"*";:NEXT:PRINT
 2240ENDPROC
 2250 REM ************************************************************
 2260DEF PROClist
```

```
2270CLS:PRINT:PRINT
2280PROCtable1:PROCtable2:PRINT:PRINT:PRINT
2290PROCtable3:PRINT:PRINT:PRINT
2300PRINT TAB(30);"SPACE PAR TO CONTINUE":AA=GET:CLS
2310PROCtable4:PRINT:PRINT:PRINT
2320PROCtable5:PRINT:PRINT:PRINT
2330 PRINT TAB(30);"SPACE PAR TO CONTINUE":AA=GET:CLS
2340PROCtable6
2350PRINT TAB(25);"SPACE PAR TO CONTINUE":AA=GET:CLS
2360ENDPROC
2370 REM ************************************************************
2380DEF PROCstore
2390CLS
2400 PRINT TAB(5,5);"Put Tape Data in Drive   1    and hit any KEY  "
2410AA=GET
2420*DRIVE 1
2430*CAT
2440PRINT:PRINT
2450INPUT "     Output File Name ";FILE$
2451 F$=FILE$+"0"
2460F=OPENOUT F$
2470PRINT#F,E1$,E2$,TM,TA,E,K
2480 PRINT#F,HR(1),HR(2),FAC
2490FOR J=1 TO 3
2500PRINT#F,C$(J),A(J),R(J),L(J)-L(J-1)
2510NEXT J
2520PRINT#F,BIOT(1,1),BIOT(1,2),BIOT(1,3)
2530PRINT#F,BIOT(2,1),BIOT(2,2),BIOT(2,3)
2540FOR I=1 TO 2
2550FOR J=1 TO 6
2560PRINT#F,C(I,J)
2570NEXT J
2580NEXT I
2590CLOSE#F
2600F$=FILE$+"1"
2610F=OPENOUT F$
2620FOR I=1 TO Z%
2630PRINT#F,Z(I),TZ(1,I)
2640NEXT I
2650CLOSE#F
2660F$=FILE$+"2"
2670F=OPENOUT F$
2680FOR I=1 TO Z%
2690PRINT#F,Z(I),TZ(2,I)
2700NEXT I
2710CLOSE#F
2720F$=FILE$+"3"
2730F=OPENOUT F$
2740FOR I=1 TO Z%
2750PRINT#F,Z(I),DTZ(1,I)
2760NEXT I
2770CLOSE#F
2780F$=FILE$+"4"
2790F=OPENOUT F$
2800FOR I=1 TO Z%
2810PRINT#F,Z(I),DTZ(2,I)
2820NEXT I
2830CLOSE#F
2840*DRIVE 0
2850ENDPROC



2860END ************************************************************
```

APPENDIX B

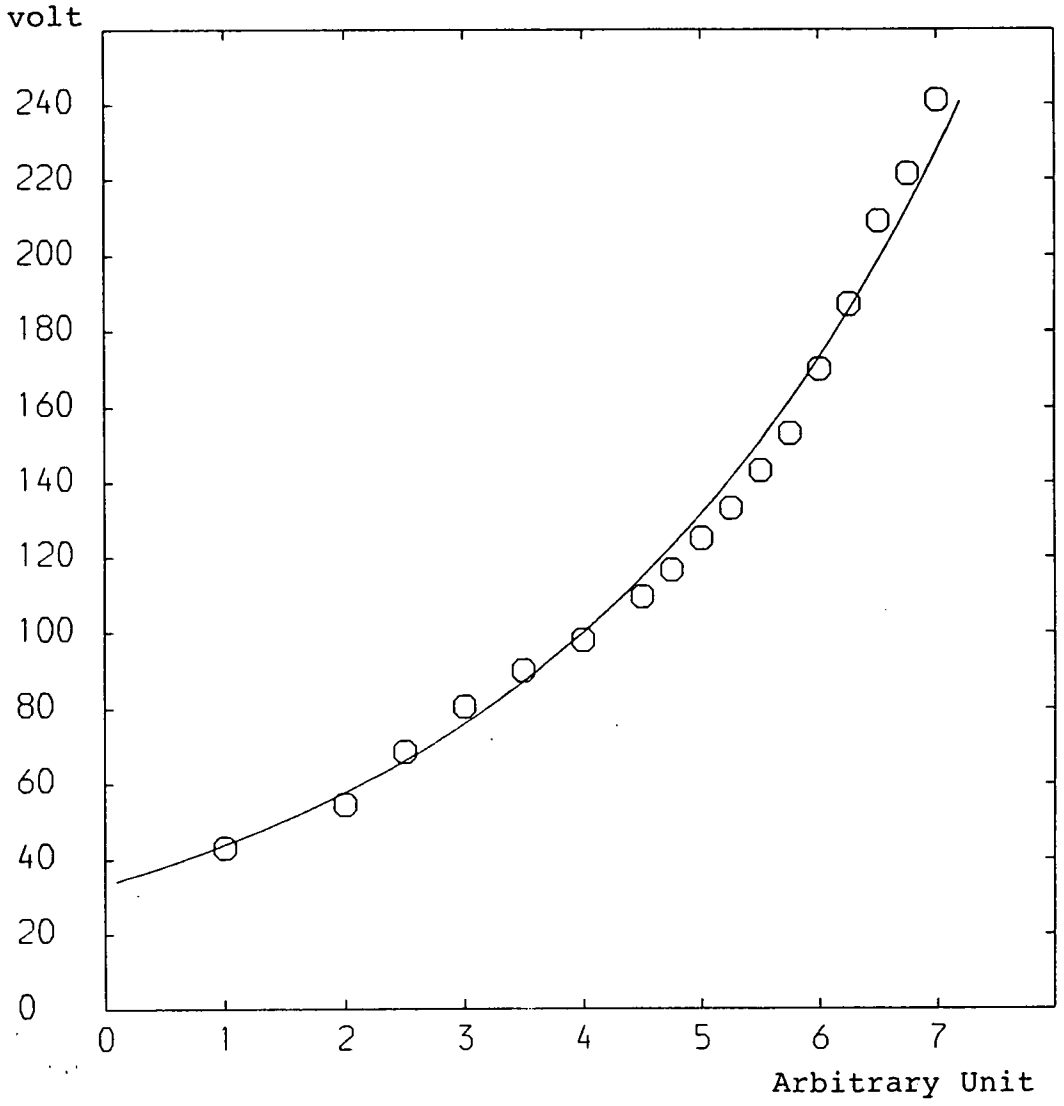

The voltage calibration curve for the R-F heating coil.

APPENDIX C

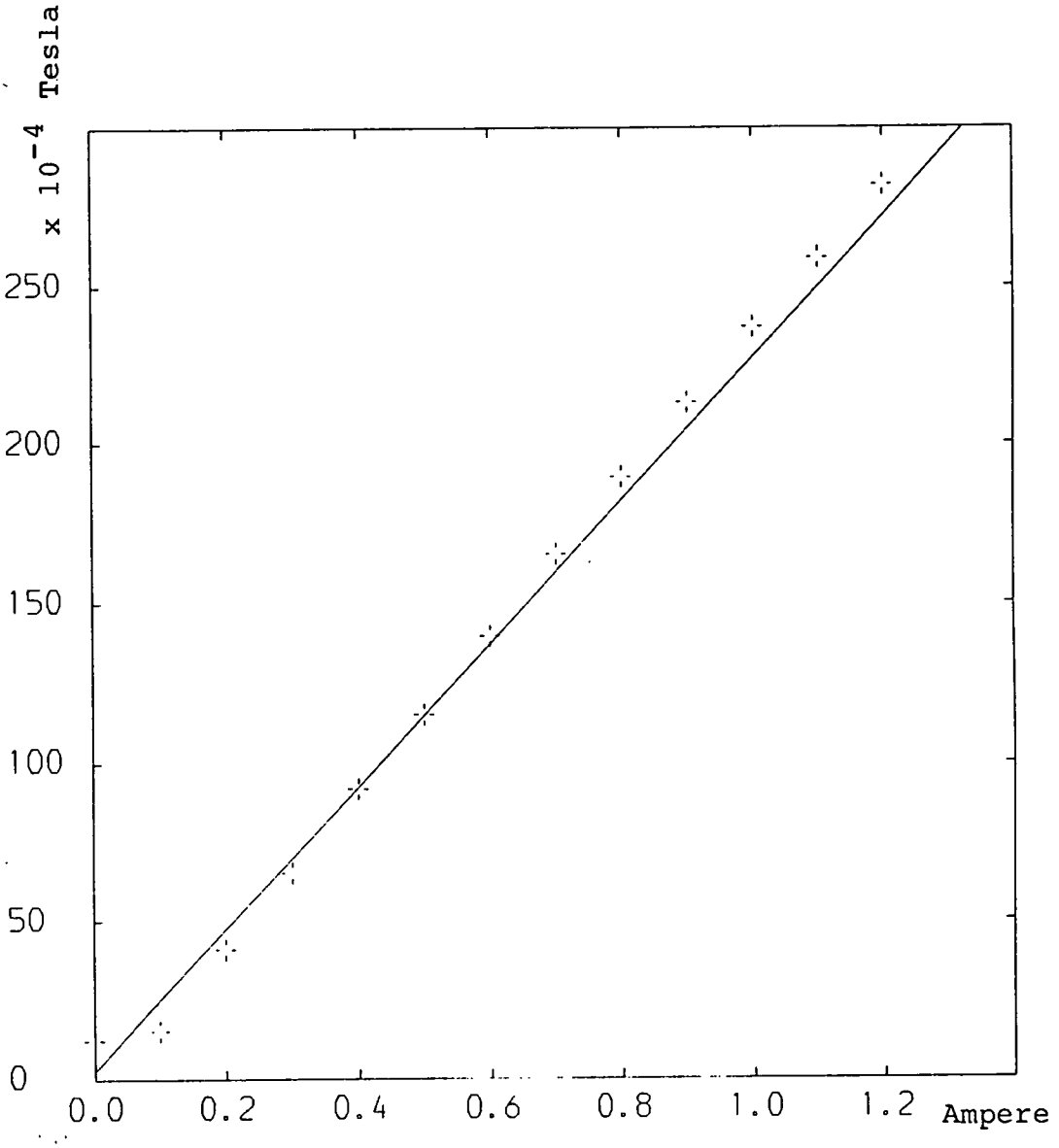

Calibration for the coil used for magnetic domain movement experiment

Austermann, J.B., Newkirk and Smith, D.K. J. Appl. Phys. 36, 3815, (1965).

Authier, A., Adv. X-ray analysis, 10, 9, (1978).

Baker, J.F.C., Hart, M., Milliveel, M.A.G., and Heckingbollom, R., Solid-State Electronics, 19, 331, (1976).

Bardsley, W., Green, G.W., Holliday, C.H., and Hurle, D.T.J., J.C.G., 16, 277, (1972).

Balchin, A.A., and Whitehouse, C.R.,

Barnett, S.J., Tanner, B.K., and Brown, G.T., Mat. res. Soc., 41, 83, (1985).

Batterman, B., and Cole, H., rev. Mod. Phys., 36, 681, (1964).

Becker, C., and Pegel, B., Phys. Stat. Sol. 32, 443, (1969).

Bond, W.L., and Andrus, J., J. Mineral. Soc. Amer., 37, 622, (1952).

Boettinger, W.J., Burdette, H.E., Kuriyama, M., and Green, R.E., rev. Sci. Instrum., 47, 906, (1976).

Brandle, C.D., Ch. 7 in "Crystal Growth", edited by Brian R. Pamplin, Pergamon Press, 1980.

Brenner, S.S. in "The art and Science of Growing Crystal", (Gilman, J.J. ed.), p. 30, John Wiley & Sons, Inc. New York, (1963).

Brice, J.C., The growth of crystals from the melt, North-Holland Publishing Company, Amsterdam (1965).

Brice, J.C., J.C.G. 2, 395, (1968).

Buckley-Golder, I.M., Ph.D. Thesis, Oxford University (1977).

Buckley-Golder, I.M., and Humphreys,C.J. Phil. Mag. A, 13, 41, (1979).

Bye, K.L., J. Mater. Sci., 14, 619, (1979).

Calverley, A., Davis, M., and Lever, R.F., J. Sci. Inst., 34, 142, (1957).

Champier, G. in "Characterization of crystal growth defects by X-ray methods", Tanner, B.K., and Keith, B.D. eds., p.116, Plenum Press, New York (1980).

Chikawa, J-I, J., J.C.G., 24/25, 61, (1974).

Chikawa, J-I, J., and Austermann, S.B., Adv. X-ray analysis, 11, 394, (1967).

Croxall, D.E., Ward, R.C.C., Wallace, C.A., and Kell, R.C., J.C.G., 22, 117 (1974).

Dash, W.C., J. Appl. Phys., 29, 739, (1958).

Dash, W.C., J. Appl. Phys., 30, 459, (1959).

Deguchi, Y, Kobuo, N., Kashiwaya, K., and Kino, T., Jap. J. Appl. Phys., 17, 611, (1978).

Kittmar, W., and Neumann, K., in "Growth and perfection of Crystals", (Doremus, R.H., Roberts, B.E., and David Turnbull eds.), P.121. New York, John Wiley & Sons, Inc. (1958).

Duckett, R.A., and Lang, A.R., J.C.G., 18, 135, (1973).

Elbaum, C., Phil. Mag., 5, 669, (1960).

Emara, S., Lawn, B.R., and Lang, A.R., Phil. Mag. 19, 7, (1969).

Fang, D.F., Xiang-Xi, W., Young-quan, Xu., and Li-Tong, Li., J.C.G., 66, 327, (1984).

Fehmer, H., and Uelhoff, C., J.C.G., 15, 195, (1972).

Fisher, G.R., and Barnes, P., J. Appl. Cryst., 17, 231,(1984).

Fiedler, R., and Lang, A.R., J. Mater. Sci., 7, 531, (1972).

Fries, E., Spendel, M., and Philibert, J. Appl. cryst. 14, 285, (1981).

Garabedian, F.G., kestigian, M., Cohen, M.L., and Von Thuna, P.C., american Ceramic Society Bulletin, 55, 726, (1978).

Gartner, K.J., Rittinghaus, K.F., and Seeger, A., J.C.G., 13114, 619, (1972).

Gatog, N.C., Ch. 1. in 2Crystal Growth: A tutorial approach", (Birdsley, W., hurle, D.T.J., and Mulline, J.B. eds.), North-Holland Publishing Co., (1979).

Goriletsky, V.I., Nemenov, V.A., Protsenko, V.G., Radkevich, A.V., and Eidelman, L.G., j.C.G., 52, 509, (1981).

Greene, L.C., and Czyzak, S.J., J. Chem. Phys. 29, 1375, (1958).

Gross, U., and Kersten, R., J.C.G., 15, 85, (1972).

Hosaka, M., and Taki, S., J.C.G., 53, 542, (1981).

Howe, S., and Elbaume, C., J. Appl. Phys., 33, 1227, (1961).

Hutchinson, F., Ph.D. Thesis, Durham University (1958).

Jones, D.W., Ch. 4., Crystal Growth Theory and Technique, vol. 1, edited by Goodman, C.M.L., (1974).

Jones, G.R., Young, I.M., Cockayna, B., and Brown, G.T., Microsc. Semicond. Mater. Conf. Oxford, p.6, (1981).

Jourdan, C., Rome-Talbot, D., and Gustaldi, J., Phil. Mag. 26, 1053, (1972).

Jourdan, C., and Gastaldi, , Scripta metallurgic 13, 55, (1979).

Kamada, K., prog. cryst. growth. charact. 3, 309, (1981).

Keck, P.H., Green, M., and Polk, M.L., J. Appl. Phys. 24, 1479, (1953).

Keck, P.H., and Colay, , Physical Rev. 89, 1297, (1953).

Kohda, H., Yamada, K., Nakanishi, H., Kobayski, T., Osaka, J., and Hoshikawa, K., J.C.G. 71, 831, (1985).

Kolb, E.P., Wood, P.L., and Laudies, R.A., J. Appl. Phys., 39, 1362, (1968).

Kuroda, E., Kozuka, H., and Takan, J.C.G. 68, 613, (1984).

Kuriyama, M., Bettinger, J., and Burdette, E., J.C.G., 43, 287, (1978).

Lang, A.R., J. Appl. Phys. 29, 597, (1958).

Lang, A.R., Acta Cryst. 29, 249, (1959).

Lang, A.R., Brit. J. Appl. Phys. 14, 9021, (1963).

Lang, A.R., and Polcarova, M., Proc. Roy. Soc. A285, 297, (1965).

Lang, A.R., p.623 in "Diffraction and imaging techniques in Material Science", eds. by Amelinckx, Geners and van Landuyt, North-Holland, (1978).

Laudies, R.A., "The growth of single crystals", Prentice-Hall, Englewood Cliffs, N.J., (1970).

Laue Atlas (Julich Nuclear Research Centre), Present, (1973).

Lawson, W.D., and Ielson, S., "Preparation of single crystal", Butterworths Scientific Publication (1958).

Lias, N.C., Grudenski, E.E., Kolb, E.D., and Laudies, R.A., J.C.G. 18, 1, (1973).

MacCormack, I.B., and Tanner, B.K., J. Appl. Cryst. 11, 40, (1978).

Merz, K., J. Appl. Phys. 31, 147, (1960).

Nes, E., and Nost, B., Phil. Mag. 13, 855, (1966).

Newkirk, J.B., Phy. Rev. 110, 1463, (1958).

Nost, B., Phil. Mag. 11, 183, (1965).

Nost, B., Sorensen, G., Phil. Mag. 13, 1075, (1966).

O'Kane, D.F., Kwap, T.W., Gulitz, L., and Bednowity, A.L., J.C.G., 13114, 624, (1972).

Okkerse, B., Philips Tech. Rev. 21, 340, (1959).

Okkerse, B., Section 6 of Handbook of Semi-Conductor Electronics, Second Edition, Price, D.B., Phil. Mag. 5, 473, (1960).

Paige, D.K., Ph.D. Thesis, Durham University, (1983).

Patel, J.R., J. Appl. Phys. 44, 3909, (1973).

Pearson, R.F., British J. Appl. Phys., 4, 342, (1953).

Pegel, B., and Becker, C., Phys. Stat. Sol. 35, 157, (1969).

Pielaszek, J., Phys. Stat. Sol. (a) 31, K95, (1975).

Pfann, W.C., and Macelburger, D.W., J. Appl. Phys. 27, 12, (1956).

Polcarova, M., and Lang, A.R., J.C.G., 18, 135, (1973).

Pruett, H.D., and Lien, S.Y., J. electrochem. Soc., 121, 824, June (1974).

Rek, Z., Acta Physica Polinica, A41, 635, (1972).

Safa, M., Tannr, B.K., Klapper, H., and Wanklyn, B.M., Phil. Mag. 35, 811, (1977).

Safa, M., and Tanner, B.K., Phil. Mag. B. 37, 739, (1978).

Schultz, J.M., and Armstrong, R.W., Phil. Mag. 10, 497, (1964).

Steinemann, A., and Zimmerli, , J. Phys. Chem. Solids Suppli., 1, 81 (1966).

Sworn, C.M., and Brown, T.E., J.C.G. 15, 195, (1972).

Tanner, B.K., Z. Naturforsch 28a, 676, (1973).

Tanner, B.K., "X-ray diffraction topography", Pergamon Press, (1976).

Tanner, B.K., prog. crystal growth 1, 23, (1977a).

Tanner, B.K., in "Surface and Defect Properties of Solid", vol. 6, 280, (1977b).

Tanner, B.K., Midgley, D., and Safa, M., J. Appl. Cryst. 10, 281, (1977c).

Tanner, B.K., and Bowen, D.K. eds. "Characterization of crystal growth defects by X-ray method", Plenum Press, (1980).

Tanner, B.K., in "Characterization of crystal growth defects by X-ray methods", eds. Tanner, B.K., and Bowen, D.K., Plenum Press p.471 (1980).

Tanner, B.K., and Smith, S.H., J.C.G. 28, 77, (1975).

Tetsuy, A., and Nobuyuki, K., Jap. J. Appl. Phys. 8, 1091., (1969).

Theurer, H.C., J. Electr. Chem. Soc. 108, 841, (1961).

Theurer, H.C., and Hauser, J.J., J. Appl. Phys. 35, 554, (1964).

Tohano, S., Shinoyama, S., Katsui, A., and Takaoka, H., J.C.g. 73, 190, (1985).

Turner, A.B.L., Vneeland, T.J.R., and Pope, D.P., Acta. cryst. 4, 452, (1968).

van der Hart, A., and Welmoff, W., J.C.G. 51, 251 (1981).

van Dirk, H.J.A., Jocham, C.M., Scholl, G.J., and van der Werf, P., J.C.G. 21, 310, (1974).

van Uitert, L.G., and Egerton, L., J. Appl. Phys. 32, 959, (1961).

Wernick, J.M., and Davies, H.M., J. Appl. Phys. 27, 149, (1956).

Zulehner, W., and Haber, D., in "Crystal growth, Properties and application", 8, 1, (1982).